10-5-2017

Energy Harvesting from Surface River/Ocean Waves

Wenzheng Cai
University of Windsor

Energy Harvesting from Surface River/Ocean Waves

By

Wenzheng Cai

A Thesis
Submitted to the Faculty of Graduate Studies
through the Department of Mechanical, Automotive & Materials Engineering
in Partial Fulfillment of the Requirements for
the Degree of Master of Applied Science
at the University of Windsor

Windsor, Ontario, Canada

2017

Energy Harvesting from Surface River/Ocean Waves

by

Wenzheng Cai

APPROVED BY:

_____

T. Bolisetti

Department of Civil & Environment Engineering

_____

G. Rankin

Department of Mechanical, Automotive & Materials Engineering

_____

V. Stoilov, Co-Advisor

Department of Mechanical, Automotive & Materials Engineering

_____

V. Roussinova, Co-Advisor

Department of Mechanical, Automotive & Materials Engineering

September 15, 2017

DECLARATION OF ORIGINALITY

I hereby certify that I am the sole author of this thesis and that no part of this thesis has been published or submitted for publication.

I certify that, to the best of my knowledge, my thesis does not infringe upon anyone's copyright nor violate any proprietary rights and that any ideas, techniques, quotations, or any other material from the work of other people included in my thesis, published or otherwise, are fully acknowledged in accordance with the standard referencing practices. Furthermore, to the extent that I have included copyrighted material that surpasses the bounds of fair dealing within the meaning of the Canada Copyright Act, I certify that I have obtained a written permission from the copyright owner(s) to include such material(s) in my thesis and have included copies of such copyright clearances to my appendix.

I declare that this is a true copy of my thesis, including any final revisions, as approved by my thesis committee and the Graduate Studies office, and that this thesis has not been submitted for a higher degree to any other University or Institution.

ABSTRACT

The renewable energy is an important subject especially today as the world is facing the results of the pollution and depletion of the conventional energy resources. Around 70% of the Earth's surface is covered by water where the energy of the waves/tides could be used as alternative source of energy that is sustainable and environmental friendly. Most of the research efforts are focused on the development of the large-scale technologies that can operate in the open Ocean. The potential of the low-frequency and small-amplitude wave condition in shallow rivers and lakes where most of the world wave energy exists has not been explored yet.

The objective of the current study is to design and develop new concepts for wave energy extraction, which depend on oscillatory wave motion and have the ability to convert the small and medium waves. The proposed devices are self-generating without any external sources, which makes them lightweight and naturally floating on the surface of the water.

Feasibility studies of both designs were performed using numerical modeling and field experiments. The final prototypes achieved power output of 5.0±0.6mW and 0.25±0.01mW, respectively. Array systems implementing both concepts were also introduced to improve the performance of the devices.

ACKNOWLEDGEMENTS

I would like to express my sincere gratitude and profound appreciation to my supervisors, Dr. V. Stoilov and Dr. V. Roussinova, for their patience, guidance, and continuing encouragement. They took their precious time to discuss all the details of the project, and shared their valuable experience in designing the convertors. Especially, their assistance in modeling the MATLAB simulation was invaluable and immeasurable, which speeded up the process of the research tremendously. It was impossible to complete this project without the instruction from them.

I would also appreciate laboratory technologists for preparing the experiment equipment and assistant in manufacturing both types of convertors, especially in soldering the electrical cable and sealing the convertors.

TABLE OF CONTENTS

LIST OF TABLES

LIST OF FIGURES

LIST OF APPENDICES

LIST OF ABBREVIATIONS

EPRI	Electric Power Research Institute
TWh	Terawatt-hour
yr	Year
kW	Kilowatt
Hz	Hertz
m	Meter
ft	Feet
cm	Centimeter
OWC	Oscillating Water Column Convertor
LIMPET	World's First Commercial Wave Power Device
OWC	Oscillating Body Convertor
MW	Megawatt
PZT	Lead Zirconate Titanate
mJ	Millijoule
PVDF	Polyvinylidene Fluoride
W	Watt
mm	Millimeter
ANSYS	Engineering Analysis Software
MATLAB	Matrix Laboratory
PTO	Power Take-off
N	Newton

GPa	Giga Pascal
MPa	Mega Pascal
ODE	Ordinary Differential Equation
GEAR	A Method to Solve Stiff Differential Equation
DAQ	Data Acquisition
CAD	Canadian Dollar

LIST OF SYMBOLS

Symbol	Description
P_{wave}	Wave Energy
ρ_w	Density of water
g	Gravity acceleration constant
H	Height of wave
c_w	Wave velocity
W_b	Total work of the buoy
F_b	Force of the buoy
Z_b	Displacement of the buoy
l_b	Length of the rod
W_h	Overall work of half wave cycle
h	Displacement of half wave cycle
θ	Angle of half wave cycle
m	Mass of enclosure
M	Heavy inertial mass
μ	Dipole moment
q	Charge
d	Distance between charges
Δx	Displacement on x direction
A_x	Wave amplitude
k	Wave vector

ω	Angular frequency
Δz	Displacement on z direction
$\vec{x}$	Position of particle from origin on x direction
$\vec{z}$	Position of particle from origin on z direction
t	Time
$\vec{F}_d$	Drag force vector
C_d	Drag coefficient
$\vec{v}_w$	Velocity vector of wave
$\vec{v}_e$	Velocity vector of enclosure
$\vec{h}$	Depth vector of water
F_s	Resultant forces of spring connection
F_{PTO}	Power take-off force
$\vec{F}_{rx}$	Resultant force vector of spring connection on x direction
$\vec{F}_{ry}$	Resultant force vector of spring connection on y direction
$\vec{F}_{rz}$	Resultant force vector of spring connection on z direction
$\vec{F}_{PTOx}$	Power take-off force vector on x direction
$\vec{F}_{PTOy}$	Power take-off force vector on y direction
$\vec{F}_{PTOz}$	Power take-off force vector on z direction
$\vec{F}_{d(y)}$	Drag force vector on y direction
$\vec{F}_{d(z)}$	Drag force vector on z direction
$\vec{F}_b$	Buoyant force vector
P	Load at the tip of PZT beam

l_p	Length of the PZT beam
E	Elastic modulus
I	Inertial mass
d_{33}&d_{31}	Piezo charge constants
g_{33}&g_{31}	Piezoelectric voltage constants
k_s	Stiffness of the spring
l_c	Spring length after tension and compression
l	Natural length of spring
C	Damping coefficient
$\Delta\vec{v}$	Velocity difference vector between the wave and the convertor
E_d	Energy from 'dumping' force
V_{wave}	Velocity of wave
m_f	Mass of buoy
F_b^b	Buoyant force of buoy
F_d^b	Drag force of buoy
$F_{x,i-1}$	Forces of strips on x direction
$F_{y,i-1}$	Forces of strips on y direction
y_i	Displacement of the buoy on y direction
x_i	Displacement of the buoy on x direction
V_b	Submerged volume of the buoy
Δv_b	Velocity difference between the wave and the buoy
A_b	Cross-section area of the buoy

y_1	Displacement of the plate on y direction
M_P	Mass of plate
F_b^P	Buoyant force of plate
F_d^P	Drag force of plate
$\Delta {v_p}^2$	Velocity difference between the wave and plate
A_P	Cross-section area of the plate
L	Side length of the convertor
W	Width of the PVDF strips
T	Thickness of the PVDF strips
L_P	Length of the PVDF strips
F	Force extracting from PVDF strips
V	Voltage of the PVDF strips
P_p	Energy output of the PVDF strips
C_p	Capacity of the PVDF strip

CHAPTER 1

Introduction

With most of the Earth's surface covered with water, waves have the potential to become environmentally-friendly energy source. Unfortunately, the wave energy has not been thoroughly explored as a renewable energy source and the technology of wave energy extraction is not fully developed. Despite of the large-scale ocean wave convertor, the small-scale wave harvesters, which are suitable for low frequency and small amplitude, are still rare. After researching the wave environment in Lake Erie and other regions, it was found that most frequent wave state has height less than 0.5m and period about 4 seconds.

1.1 Objectives

The main objective of this research was to develop two small-scale wave energy convertors, to take advantage of small and medium wave power. Both convertors utilize the piezoelectrical generators to convert the periodic and oscillatory wave motion into electrical power. An array energy harvesting system were designed to increase the overall power output of the convertors.

1.2 Water Wave Energy Resources

Water waves are caused by the winds as it blows over the surface of the ocean, lakes and rivers. Since majority of the Earth Surface is covered by water, water waves contain tremendous energy potential as the wind provides continuous waves along the shoreline.

Wave energy potential was typically given in terawatt-hours per year based on the recent analysis from Electric Power Research Institute (EPRI). EPRI estimated that

the total wave energy was 2,640TWh/yr which was an enormous potential and can supply with power 94,000 U.S homes for 2,600 years (Jacobson , 2011). Meanwhile, EPRI indicated that the overall recoverable wave energy resource in the U.S was 1,170 TWh/yr covering one third of electricity usage in the U.S annually (Jacobson , 2011). Table.1 shows the recoverable wave energy resource for each region.

Table 1. Recoverable wave energy for each US region (Ocean Wave Energy, n.d.).

Region	**Recoverable Wave Energy (TWh/yr)**
West Coast	250
East Coast	160
Gulf of Mexico	60
Alaska	620
Hawaii	80
Puerto Rico	20

1.3 The Great Lakes Water Wave Energy and Climate

The Great Lakes make up the largest body of fresh water on Earth and it is estimated that the wave energy potential that can be harnessed annually on average is 3-5 kW/m. Based on the report by Hawley and Eadie (Hawley & Eadie, 2007), the mean wave height along the shoreline of the Great Lakes was less than 1ft (0.30m) with wave period approximately 3 seconds (0.33Hz) which was measured during the year of 2004-2005 in Lake Erie.

Waves contain potential and kinetic energy given as

$$P_{wave} \cong \frac{1}{4}\rho_w g H^2 c_w \text{.....(1)}$$

In Eq.1, the wave energy is proportion to the square of the wave height (H) and velocity (c_w). While larger wave height and frequency provide more wave energy as predicted by Eq.1, most of the wave energy exist in small and medium wave condition. Fig.1 shows the distribution of the wave amplitude vs. wave period for the wave climate measured at Lake Erie at station 14 located at latitude 42°N and longitude 81°W. The figure points that more than 60% of the wave energy is concentrated in waves with height smaller than 30cm and frequency between 0.3 and 2 Hz (Lake Erie Physical Data Sets, 2004).

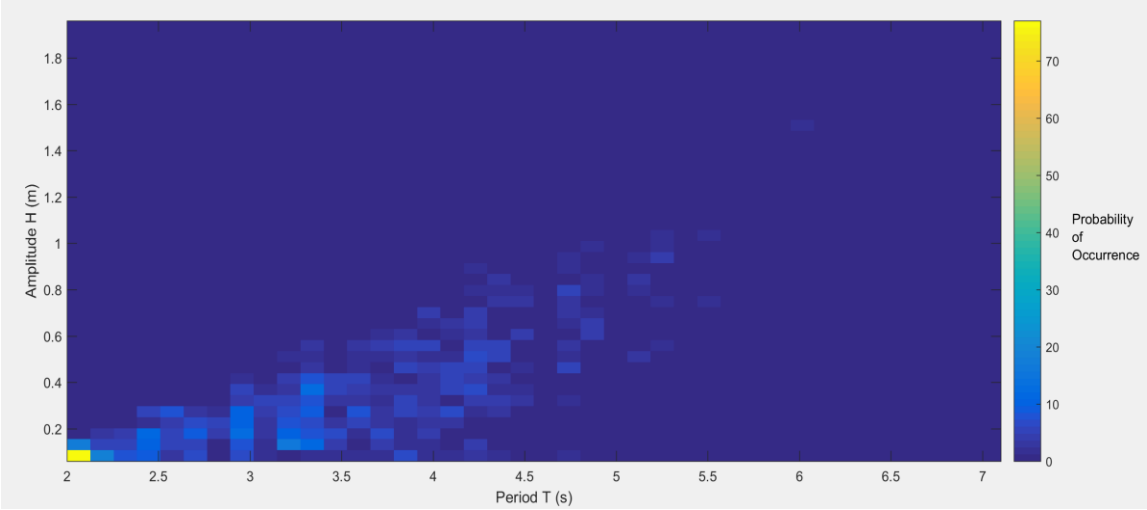

Figure. 1 Water wave energy distribution at Lake Erie station 14 (Lake Erie Physical Data Sets, 2004).

Fig. 2 presents the distribution of wave energy at Lysekil, Sweden located at latitude 58°N and longitude 11°E (Li, Isberg, Engstrom, Waters, & Leijon, 2015). At these sheltered locations, the maximum probability occurs when the wave height is lower than 0.5m and period is between 1s and 3s, which is similar to the wave environment at Lake Erie.

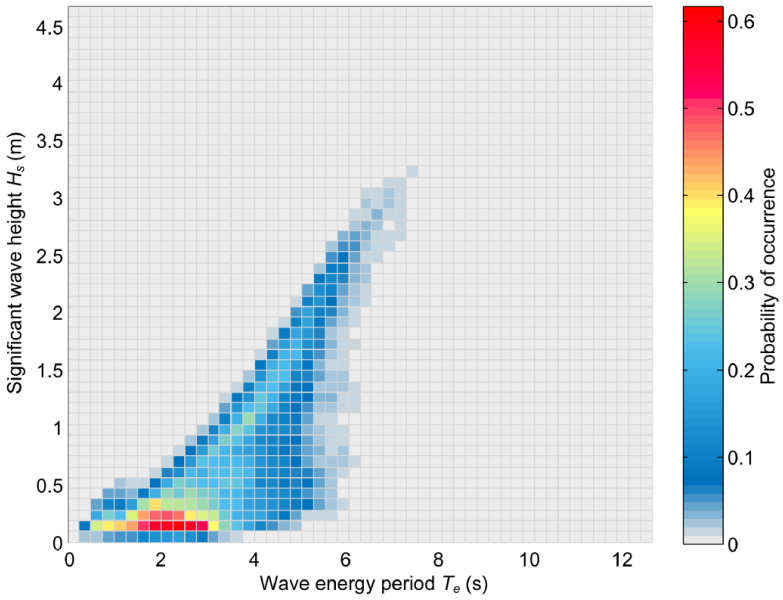

Figure 2. Water wave energy distribution at Lyskil Sweden (Li, Isberg, Engstrom, Waters, & Leijon, 2015).

The global distribution of wave energy density is also shown in Fig. 3. It indicates that the annual mean power density in most regions is lower than 50 kW/m. In other words, the majority of wave energy exists in medium and low wave environment.

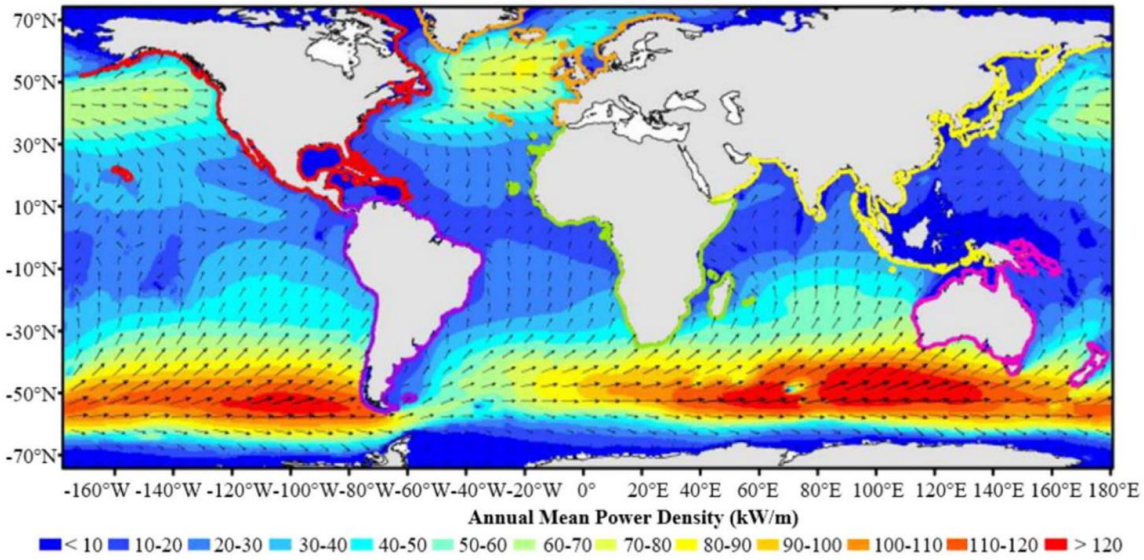

Figure 3. Global distribution of wave energy density (Mustapa, et al., 2014)

From Figs. 2 and 3, one can conclude that the small wave environment exists not only in Lake Erie but also in other locations throughout the world, which suggests the need for small-scale wave convertors have potential to be popularized globally.

1.4 The Nature of Water Wave Energy

The main benefits of wave energy are renewable and environmentally friendly since it will never run out and creates harmful byproducts. As long as the wind blows with enough consistency and force, the waves will be created along the shorelines and they will contain energy that can be harnessed. Unlike fossil fuels and nuclear energy, which will be depleted soon, wave energy can provide steady and continuous power generation. Without discharging gas, waste and pollution, wave energy does not contaminate the environment, and does not contribute to the greenhouse effect which adversely affects the climate. Another motivation of using wave energy is enormous energy potential. Greentumble (Greentumble, 2015) pointed that the energy density of waves along shorelines was around 35 kW/m, and this value could be even bigger to 100 kW/m further out into the ocean.

There are variety of devices which can extract energy from the waves. They can be classified according to the principle of operation as terminator devices, attenuators, point absorbers and overtopping devices. These technologies have been developed as prototypes worldwide to harvest wave energy and produce electricity to families, factories and commercial purpose. However, current high cost of investment and construction has become one of the toughest challenges. Most wave energy harvesters are still in the developmental stage and require huge amount of funds for maintenance. All these devices must be exposed to oceanic conditions for a long time, which could cause damage to the equipment. For example, the seawater results in corrosion on the

surface of the metal, and the storms may destroy the wave devices. Even though the wave energy is considered clean, it still can have a negative effect on marine ecosystem. Large wave convertor systems, built near shoreline, make noise that disturbs the sea life around this region. The operation of wave devices may change the direction of water flow and disturb seafloor, which could impact on the habitat of marine life and fish.

CHAPTER 2

Literature Review

This chapter provides an overview of the relevant literature and summary of the research on the energy harvesting from water surface waves. The literature review is divided into two main sections. The first section presents three mainstream concepts, which are widely researched and technologically adopted for generating electricity from waves. The second section reviews various designs and experimental results related to the use of the piezoelectric wave generators.

2.1 Three Mainstream Concepts

Wave energy harvesters capture the energy exciting in water waves to produce electrical power. As mention in previous chapter, there is a variety of wave energy technologies used to absorb energy from waves. These technologies and concepts can be developed according to the location and the water depth. Three mainstream concepts are technologically adopted to generate electricity from the wave motion and still subject of continuing research. These are: oscillating water column (OWC), oscillating body convertors (OBC) and overtopping convertors. In what follows some details for each of these technologies are discussed.

2.1.1 Oscillating Water Column

Oscillating water column (OWC) convertor is a shoreline wave energy device. It is built on rocky shores or near to cliffs next to a deep-sea bottom with a consistent and strong wave climate.

The fundamental principle of these devices is converting the wave energy into air pressure and flow which drive a turbine generator. The conversion devices are developed with a semi-submerged chamber fixed directly at the shoreline. The chamber

used to keep a trapped air pocket above a column of water in a closed structure, that could be a man-made duct or a natural cave (Wave Energy Devices, n.d.). An air-turbine generator is positioned above the waters surface as shown in Fig.4.

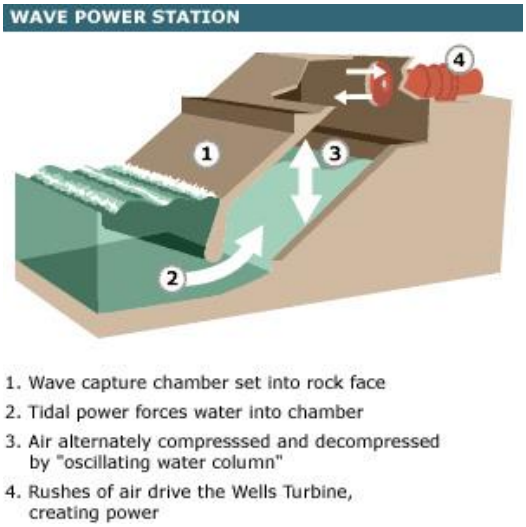

Figure 4. Oscillating water column (OWC) convertor (Wave Energy Devices, n.d.)

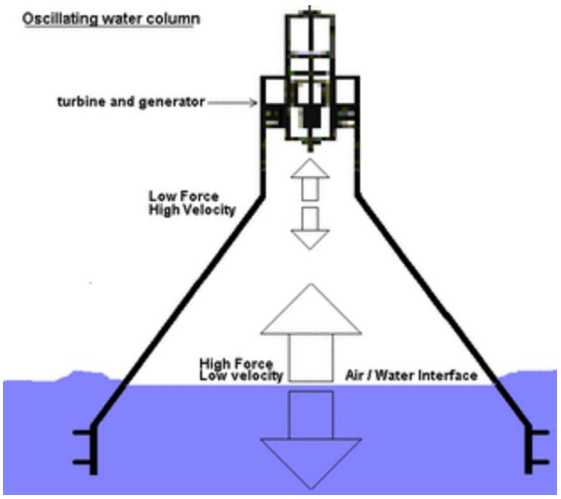

Figure 5. Alternative structure of OWC (How Hydrokinetic Energy Works, 2008)

Fig.5 presents an alternative structure with a turbine which is built perpendicular to the waves. The chamber keeps part of the water surface trapped inside with air above the surface. Below the water line, it is open to the sea. The water inside the structure is forced to move up and down by the constant flowing and oscillating motion of the wave.

With the waves enter and exit the chamber, the water level within the chamber begins to oscillate in the vertical up and down direction. The water column inside the enclosure acts like a piston which moves up and down, and pushes the air out of the structure and back into it. Through this continuous movement, the air is compressed and decompressed every cycle. A reversing stream of high-velocity air is channelled through a turbine generator to produce electricity (Wave Energy Devices, n.d.).

The LIMPET-an oscillating water column convertor, which is located on the coast of Islay, Scotland, is operating as a prototype at 75kW. However, according to the research of Lemay (Lemay, 2010), the maximum capacity of the LIMPET is 500kW. In India, there is a nearshore OWC operating at 150kW. Oceanlinx built the Mk3-PC in Australian, which has the power output at 2.5MW. The generating capacity makes the OWC economically viable and competitive in the commercial market. The wave energy used to produce electricity is currently quite expensive due to installation, technology development and maintenance resulting at 14 cents per kWh according to Lemay's research (Lemay, 2010).

OWC is an environment friendly energy harvester. However, compared with other convertors developed in the ocean, the OWC does not perform as great as other renewable devices in the aspect of environmental impacts. There is a life cycle assessment of the OWC convertor indicates that the carbon emissions over 25 years would be 24 grams of carbon dioxide including construction, installation and operation (Kempener & Numann, 2014). The main advantage of this system is simplicity since the shoreline scheme is fixed other than the air turbine, which can be easily removed for repair or maintenance. Meanwhile, with deep sea installation, the OWC has possibility to operate as a reef which will increase the marine species in a specific area. The disadvantage though is uncertainty of wave environment, since the wave period

and amplitude are difficult to control. The OWC power output relies on the level of wave energy, including amplitude, speed and frequency, which vary according to the season.

2.1.2 Oscillating Body Convertor

There is another class of wave energy devices named Oscillating Body Convertors (OBC). Most part of the convertors consists of buoy floating on or near to the water surface. The buoy heaves due to the movement of the incident wave. For submersible devices, this motion is caused by the variation of the underwater pressure and absorbing the wave energy in all directions in response to the shape and motion of waves at or near the water surface. The wave energy is achieved through four motions - vertical motion, which is under the influence of gravity, horizontal motion in the direction of moving waves, pitch or yaw motions. In most cases, the combination of all four motions is involved in extracting wave energy. In order to take advantage of the force generated by the wave, some kind of force reaction is necessary to be added, which allows the forces created by the waves on the float to react against some kind of fixed resistance. Therefore, a reaction point is introduced, which might be inertial masses such as heavy plates, sea-floor anchors or a fixed dead weight (Kempener & Numann, 2014).

One type of the Oscillating Body Convertor is called a point absorber, which is a very small device compared to the periodic wavelength. If the physical size of the device profile is larger than the periodic length of the wave, this type of convertor is known as linear absorber. These two types of devices are shown in Figs. 6 and 7. The way to convert the wave energy between the reaction point and absorber results in the main difference between them. The wave energy can be generated either by a linear floating body or an oscillating system with solid parts or water itself.

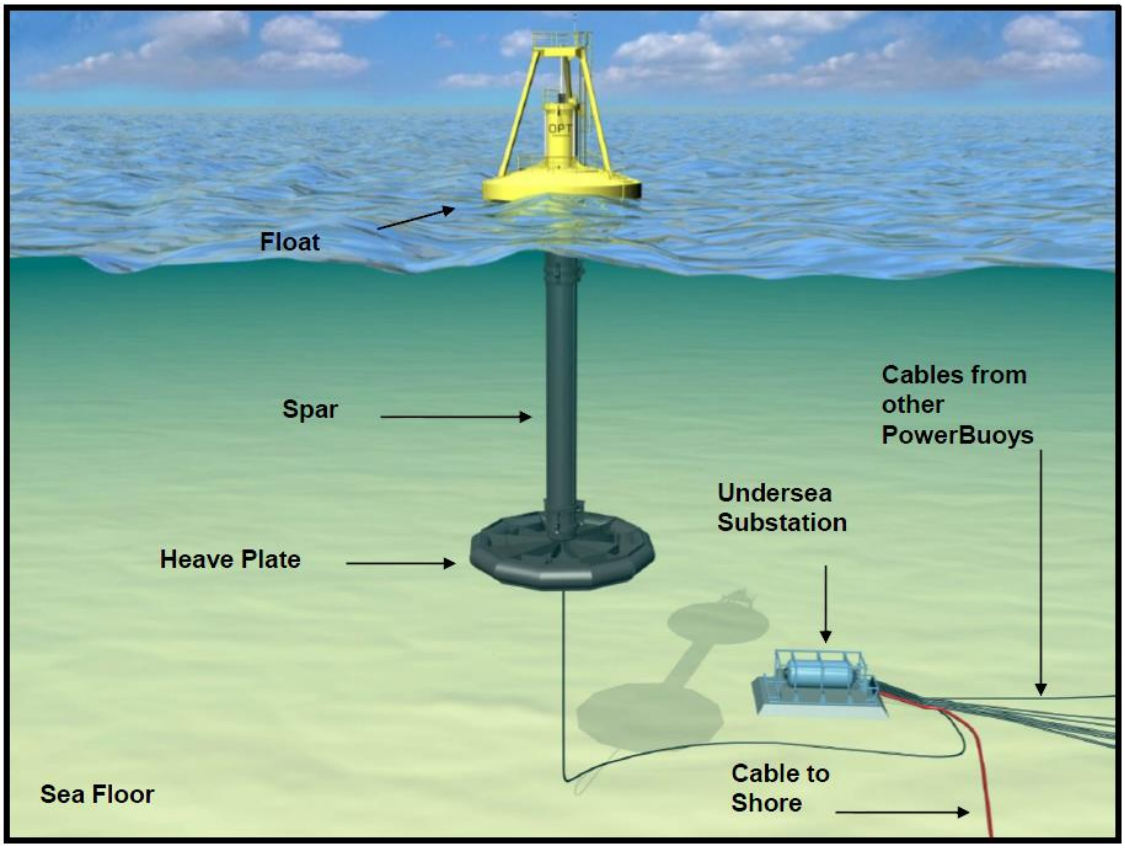

Figure 6. Oscillating body convertors (PB3 PowerBuoy , n.d.)

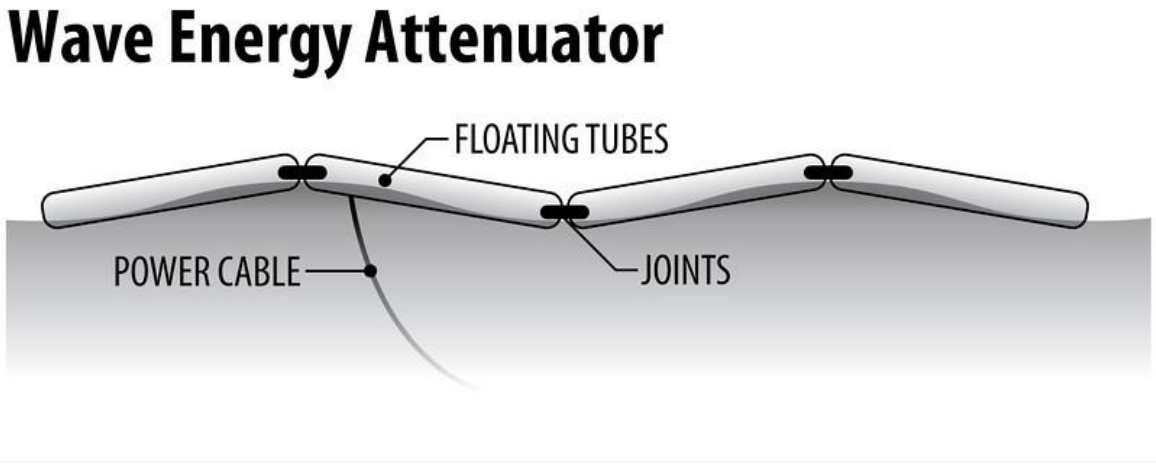

Figure 7. Wave energy attenuator (Wave Energy Attenuator, n.d.)

For the point absorber, a relative motion between the absorber and reaction point is affected by the pitching and heaving of the waves. It has a heave plate suspended below the float with spar. The entire system is attached to an undersea substation by a mooring line, which allows the device to operate offshore in deeper water, to be prevented from floating away (Wave Energy Devices, n.d.). With the up-and-down motion of the float in the waves, a hydraulic pump between the freely moving absorber and plate drives a generator to produce power, which is caused by an oscillatory mutual force reaction in between. Another type of point absorber is presented in Fig.8. It operates in an similar manner as the previous device, but is anchored with sea bottom without the mooring line, which means the freely moving buoy reacts against a fixed reaction point. As there is a fixed dead-weight on the ocean floor, these devices can operate in shallow near shore locations.

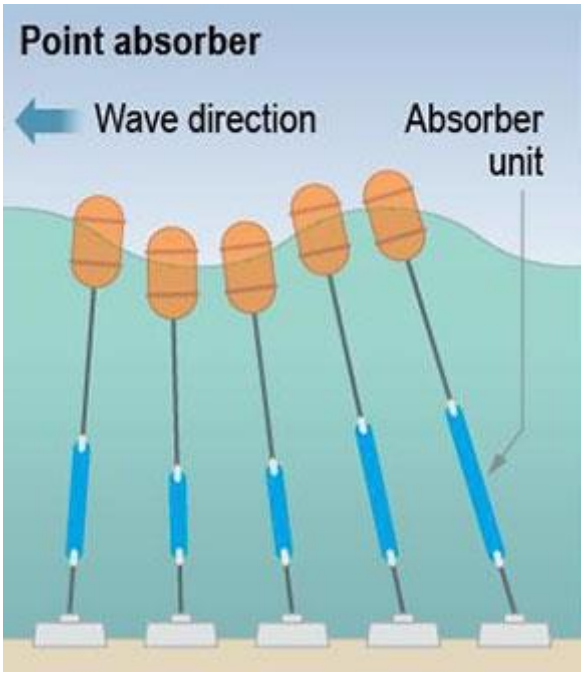

Figure 8. Point absorber (Marine and Hydrokinetic Technology Glossary, n.d.)

The linear absorber usually floats on the surface of the water. Basically, these devices consist of power cable, floating tubes, joints and hydraulic motors. In order to

swing vertically towards the incoming waves, it is attached to the ocean floor with power cable. In response to the shape of the wave, the long cylindrical bodies, which are connected by joints, sag downwards in the trough of wave and arch upwards on the crest of a wave as the waves pass along the length of the device. With the relative motion between two floating tubes, the connecting joints flex in the waves bringing about a force. A hydraulic ram at each joint is trigged by the force to drive a hydraulic motor producing the power.

FO3 concept is a commercial point absorber developed by Norwegian entrepreneur Fred Olsen. It has several heaving floaters attached to a 36m × 36m base providing the power up to 252 MW (Wave Energy Converters, n.d.) Comparable, the Wave Star with numbers of floaters on movable arms, operated by Wave Star ApS, has capability of producing energy of 6MW at full scale (Wave Energy Converters, n.d.) The major benefit of oscillating body convertors is versatility since most part of the systems naturally floats on the water surface, which means they are able to apply either near shore locations or in the open ocean.

2.1.3 Overtopping Convertor

The overtopping wave convertor is a near shore wave power device, which converts the movement of waves into potential energy as shown in Fig. 9. The principle of capturing the wave is lifting water up onto a holding reservoir above sea level which creates a low head situation. The electricity is generated by draining the higher-level water out through a conventional low head hydro turbine (Kempener & Numann, 2014)

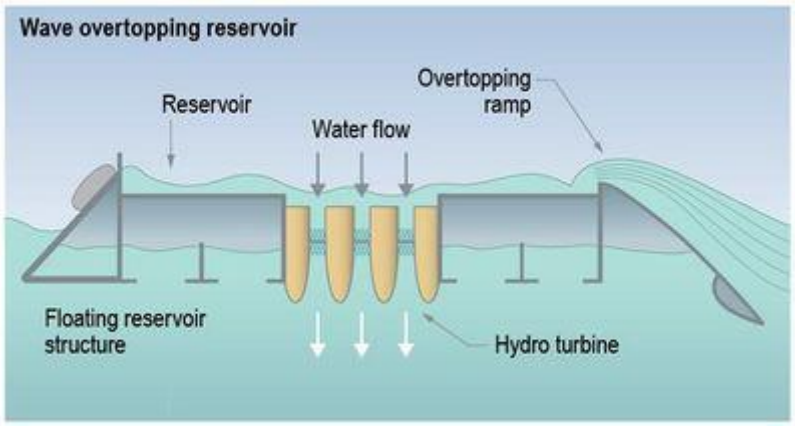

Figure 9. Overtopping wave convertor (Marine and Hydrokinetic Technology Glossary, n.d.)

The overtopping convertors consist of either bottom fixed or a floating impoundment structure and usually use reflecting arms to ensure that the waves spills over the top of a ramp design and elevate the incoming waves above the sea level. As waves arrive, they are captured and restrained into a raised water impoundment reservoir. The potential energy of water, due to the height of trapped water above its natural height, is transformed into electricity power via a turbine generator as the water returns to the sea.

Compared with oscillating water column devices and oscillating body convertors, the overtopping convertors have lower power output as the efficiency of low head hydro turbine and they are design for only deep-water shoreline and low tidal range (Wave Energy Devices, n.d.). Although some floating offshore capture devices have been developed to solve the limitations, they rely on sufficient water power. It needs to stand the test of hard weather condition, such as the forces of tides and strong storms. Maintenance and repair could also raise the cost despite the low efficiency of the generator with only about 30%. However, the main advantage of this system is

simplicity – it produces power until it stores enough water. Some commercial representative devices, such as WaveCat and Wave Dragon are shown in Fig. 10.

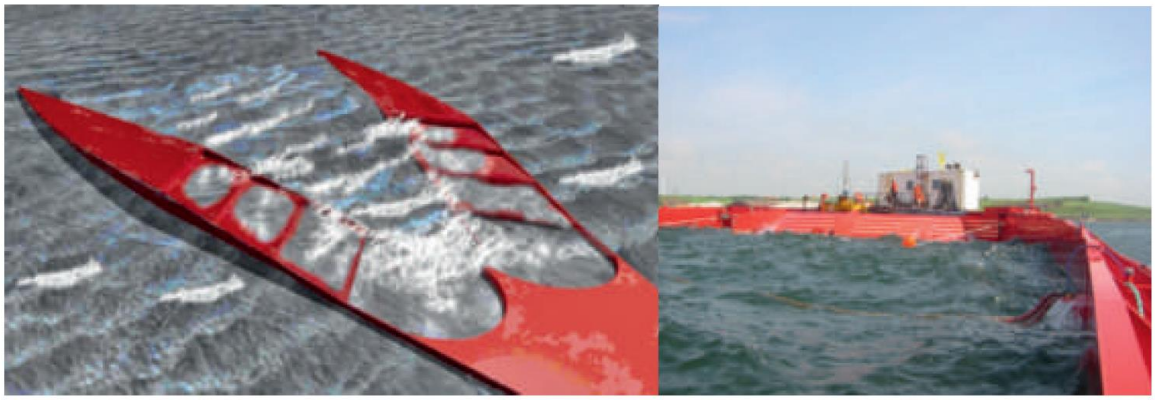

Figure 10. WaveCat and Wave Dragon (Kempener & Numann, 2014)

The reason why these three concepts were selected for review was that they are three mainstream concepts in the field of wave energy harvesting, which were commercialized. Through understanding their characteristics and comparison between big-scale and small-scale convertors, it helped to realize the advantages and disadvantages of the two potential concepts.

2.2 Piezoelectric Wave Convertor

In this section, some piezoelectric wave convertors are reviewed. The piezoelectric generator has been used in the small-scale wave convertors. It has capability of capturing waves with low frequency and small height and producing appreciable electricity.

2.2.1 Disk Piezoelectric Wave Generator

The disk piezoelectric wave generator is a deep-sea and low-consumption device using low-cost disk piezoelectric elements. The basic structure of design is shown in Fig.11. Four identical piezoelectric disks are attached to enclosure, and

impacted at their center by two spherical masses. A balance-like physical pendulum was designed to connect two masses. The disk piezoelectric elements were built from lead zirconate titanate (PZT) material with diameter of 1.5cm and response frequency of a few kHz. Two different mooring configurations were developed to maximize the output efficiency affected by the kinetic and potential energy, which was related to the movement of wave (Vinlol, Toma, Manuel, & Rio, 2013)

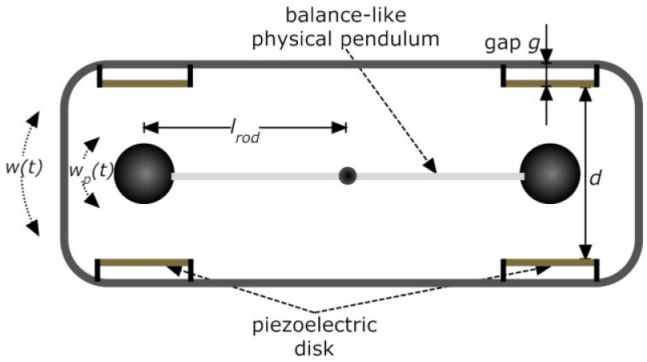

Figure 11. Disk piezoelectric wave generator convertor system (Vinlol, Toma, Manuel, & Rio, 2013)

In Fig. 12, the mooring configurations for sea heave motion, which took advantage of the vertical movement of a floating body is shown. The energy convertor system was attached to the buoy with a mooring line, which provided upward and downward motion of the enclosure. With the pulling force created by the wave, the spherical masses along with the pendulum system started to swing freely, which caused the continuous impacts on the piezoelectric disk. In order to create a pull-down force at the other side of the box, a heavy weight was added on the opposite side of the mooring line with a floating body. The total work done the motion of buoy could be calculated:

$$W_b = F_b * Z_b \text{.....(2)}$$

$$F_b = \frac{1}{4} * \rho_w * g * \pi * {Z_b}^2 * l_b \text{.....(3)}$$

where W_b is the total work of the buoy, F_b is the force of the buoy, Z_b is the displacement of the buoy, and l_b is the length of the rod

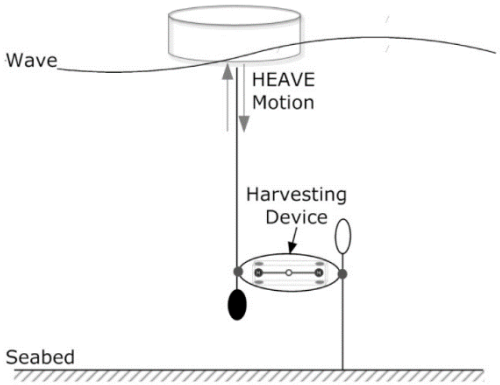

Figure 12. Mooring configurations for heave motion (Vinlol, Toma, Manuel, & Rio, 2013)

Since the waves induced the buoy to heave, the oscillating pitch motion occurred on the harvesting device. Unlike the previous configuration shown in Fig. 12, the enclosure itself was designed as a buoy attached to the seabed directly with a mooring line as shown in Fig. 13. In this case, the pendulum system experienced a reversal movement against the wave motion since the gravitational axis of enclosure remained perpendicular to the wave surface that created an angular displacement of the harvesting device, and the mass difference between enclosure and spherical inertia leaded in a delayed motion of the masses. In a complete wave period, the piezoelectric elements were impacted by the spherical masses due to the oscillating movement of the

device itself. The overall work done for a half wave cycle was presented in the equations below.

$$W_h = m_b * g * h \text{.....(4)}$$

$$h = H * (1 - \cos(\theta)) \text{.....(5)}$$

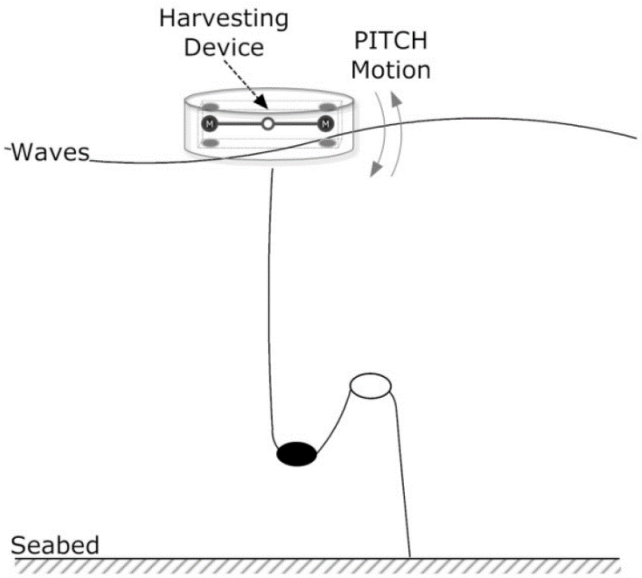

Figure 13. Mooring configurations for pitch motion (Vinlol, Toma, Manuel, & Rio, 2013)

The conversion efficiency of the harvesting device was only 0.8%, even with heavier spherical masses. The output efficiency was only between 0.7% and 0.8% with a 23cm wave height and wind speeds varying from 0 to 3m/s. The total amount of electrical energy harvested during a 24 - hour experiment was 435Mj (Vinlol, Toma, Manuel, & Rio, 2013).

2.2.2 Piezoelectric Cantilever

The piezoelectric cantilever has been used in two water wave harvesting applications. The first application utilized the longitudinal motions of water particles

induced by the wave which created a deformation of the cantilever beam. The cantilever substrate was anchored at seabed attached with piezoelectric patches which had piezoelectric properties of polyvinylidene fluoride (PVDF) which is flexible, and a proof mass was fixed at the other side of cantilever to catch the longitudinal wave motion (Xie, Wang, & Wu, 2014) The schematic of the piezoelectric wave convertor is shown in Fig. 14. The mass has a displacement followed by the periodic and oscillatory motion of the wave, which caused in the deformation and deflection of the piezoelectric patches. With the deformation of the piezoelectric, the electrical energy was collected owing to the electromechanical coupling effect.

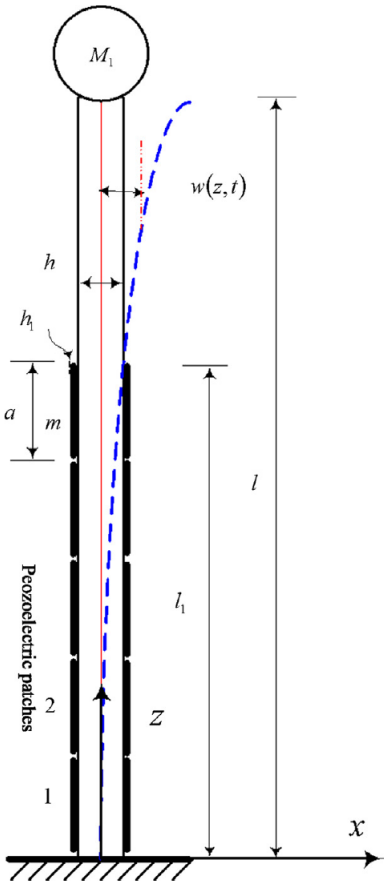

Figure 14. Schematic of the proposed energy convertor. (Xie, Wang, & Wu, 2014)

A mathematical model was developed to estimate the output power at different geometry (Xie, Wang, & Wu, 2014). It indicated that the average power output of this design has rising tendency with increase in the wave height and the sea depth. The maximum electrical power per device was estimated as 145W for the wave height of 3m and sea depth of 6m.

Since the water waves induced not only longitudinal motion but also vertical up and down motions, a modified piezoelectric wave convertor was proposed (Woo, et al., 2015). A schematic of such piezoelectric wave harvesting system is shown in Fig.15. Instead of using a convectional vibration system with vertical piezoelectrical cantilever, this wave harvester utilized the movement of a floating body attached to the free end of a piezoelectric cantilever (PZT) which was placed parallel to the water surface. The floating body was subjected to a heave motion due to the movement of the wave, which created the deflection at the free end of the cantilever. In this way, the motion of wave has been converted into mechanical energy causing the strain of the piezoelectric cantilever. Though the piezoelectric effect, the strain deformation was further transferred to electrical power successfully (Woo, et al., 2015).

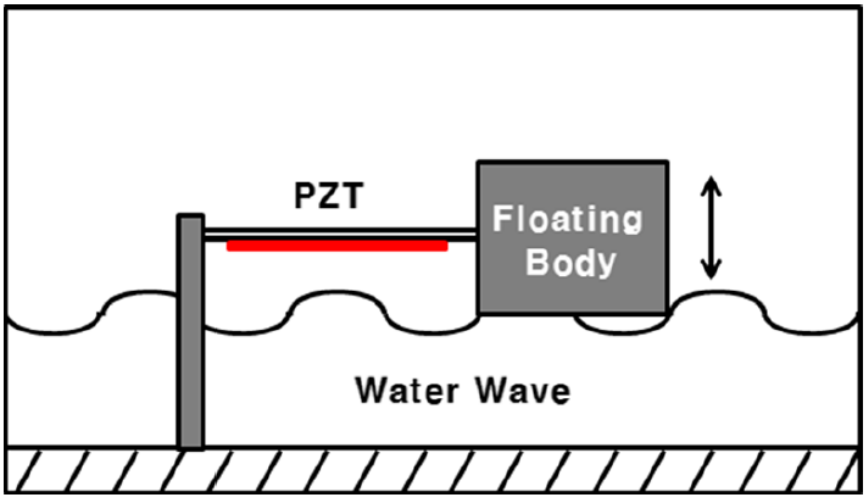

Figure 15. Schematic diagram of piezoelectric energy harvester (Woo, et al., 2015)

The research studied in the relationship between the energy output and features of piezoelectric cantilever. The harvesting system was excited with an external vibration with regular frequency in the range of 5 - 40 Hz, and the displacement at the tip of cantilever was controlled between 1 - 4 mm (Woo, et al., 2015). The first experiment analyzed whether the changes of displacement under different frequency affected the power output. The amount of output rose with the increased displacement, which meant the larger strain energy, the more power generation. To investigate the influence on electrical output with different thickness of piezoelectric generators, five piezoelectric cantilevers were vibrated at frequency from 5-40 Hz with a constant displacement of 4 mm (Woo, et al., 2015).

For the second experiment, since the displacement was kept constant, thicker piezoelectric element was used which has more strain energy. Under the same condition as the previous experiment, increasing strain energy produced more electrical power. The thickest piezoelectric cantilever had the largest energy output of 18 mW with 40Hz frequency, which was almost nine times higher than the thinnest piezoelectric (Woo, et al., 2015).

In was indicated in this study that the amount of electrical power generation depends on the displacement and strain of the piezoelectric cantilevers. Larger displacement and strain caused more power harvested.

CHAPTER 3

Design of The Wave Energy Convertors

In this chapter, the details of two new wave energy concepts - an Acceleration-based convertor and a Deformation-based convertor are presented. In Section 3.1, the fundamental design and basic structure for both design principles are explained. In the meantime, the network (array) system is also introduced in section 3.2, which improves the power output from the small-scale harvesters.

3.1 Two Potential Concepts

As mentioned in Chapter 1, over 60% of wave energy exists in the environment with small amplitude and low frequency in Lake Erie and another region. To take advantage of the wave energy, two small scale wave convertors are intended to accommodate the wave energy with amplitudes from 1cm to10cm and frequencies from 0.2Hz to 1Hz.

The proposed concepts for both small-scale wave convertors rely on converting mechanical energy of the wave motion/acceleration into vibrational (strain) energy. As the water is displaced under the oscillatory wave action, the fluid particles have longitudinal and lateral movement with varied acceleration and displacement. Due to this periodical motion, the water waves contain mechanical energy. Once the convertors are subjected into water, they will follow the motion of the wave, and the energy of the wave will be transferred as mechanical energy of the convertor. The acceleration and displacement of the convertors bring about the potential and kinetic energy This process converts the oscillatory nature of water waves into mechanical (potential and kinetic) energy. This energy of the convertors is further converted into electricity by using multiple piezoelectric generators.

3.1.1 Acceleration-Based Convertor

The acceleration-driven convertor is designed to naturally float on the water surface, and does not require anchoring. The convertor has a clear box as the enclosure, and a heavy mass is located at the middle of the enclosure. The piezoelectric generators are attached on the surface of the enclosure. Between the convertors and heavy mass, there are spring connections. As a small-scale device, it has the capability of extracting energy from small-height and low-frequency waves. This is because the small-scale device will have enough displacement and acceleration to produce plenty of electrical power when it is subjected into wave. The fundamental working principle of the convertor is based on the displacement and acceleration of a heavy inertial mass inside the enclosure. Fig. 16a illustrates the general idea of operation of the convertor. Triggered by the motion of the wave, the floating enclosure with mass (m) starts to accelerate. The motion of the wave provides a lift (buoyancy) force on the enclosure with an upward motion. Consequently, the heavy inertial mass (*M*) inside follows the motion with delay and much smaller acceleration.

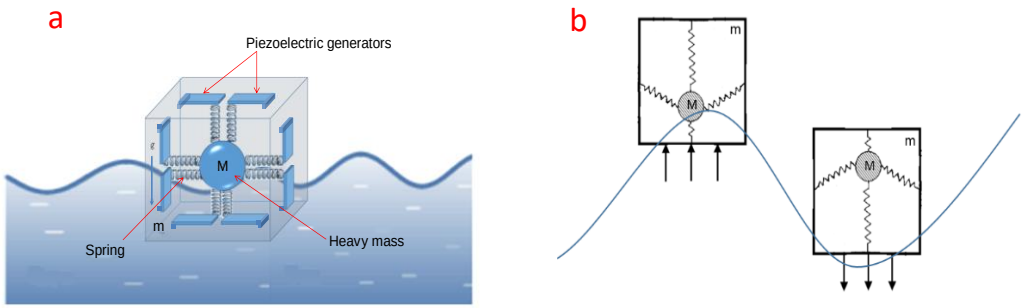

Figure 16. (a) 3-D diagram of the Acceleration-based convertor system (b) 2-D diagram of the Acceleration-based convertor system

The difference in the acceleration between the two masses *m* and *M* creates the necessary displacement to trigger oscillations of the two masses connected with springs as shown in Fig. 16a. The ends of the springs are connected to number of piezoelectric generators. The relative motion of the inertial mass and the enclosure results in tension/compression on the springs, which transfer the load on the tip of the piezo electric beams, resulting in strain energy. Thus, the wave energy of the slow, random and low-frequency wave motion is converted to strain energy. The 2-D schematic of the acceleration-driven convertor is shown in Fig. 16b. As it shows, the convertor follows the motion of wave as the shape of sine and cosine function periodically. This allows the heavy mass to have the same motion in opposite direction due to significant mass difference between heavy mass and enclosure. As the heavy mass moves it deforms the springs. This creates continuous bending of the piezoelectric generator that produce electricity. The principle of the piezoelectric generator will be explained in the next chapter.

3.1.2 Deformation-Based Convertor

In shallow water, there is a change in the orientation of the flow along the depth of water developing the energy distribution and the generation of longshore currents. Each part of the wave travels with different direction and velocity depending on the depth since the motion of wave is affected by the bed. The motion of incident wave and the current form velocity gradient along the depth of water and provides impact forces at the same time. Since the PVDF is a flexible material and can be easily deformed due to its small stiffness, the PVDF strips will have large deformation with face and length shear occurring periodically due to the velocity gradients, along the flow depth. The flow current also produces forces along the length of the strips, which makes the PVDF strips to either extend or compress. Meanwhile, the floating buoy attached to the strips

helps in enlarging the deformation of the strips since the buoy foam has larger volume contacting the water resulting in more reflection from the water motion. This reflection drives the PVDF strips to deformed along each direction. In this situation, plenty of strain energy will be created and converted into electric power through piezoelectric effect.

From the appearance of deformation – based convertor, it looks like a jellyfish shown in Fig. 17a with piezoelectric film strips (PVDF) as tentacles and a plate as the body. In Fig. 17b, there are 16 holes in total drilled on the plate, which allows the cable of piezoelectric generators to pass through. Those cables eventually connect to the data acquisition terminal used in the experiments. The black part in the figure is a plastic cap, which is attached to the position of those holes on the plate by glue. The purpose for the plastic cap is to hold dielectric grease which isolate the electric component from the water when the whole body of convertor is submerged. Silicon is also applied on the gap between the cap and plate to protect the electrical part. The PVDF strips are inserted through the caps and holes, and the floating foams (green parts) are attached to the strips providing enough buoyancy making the harvester float on the surface of water.

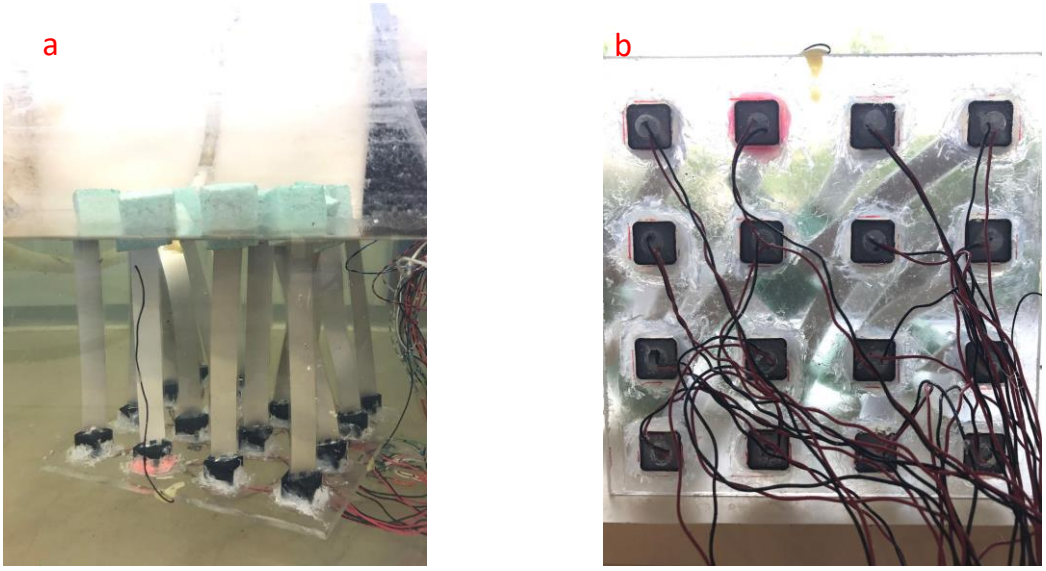

Figure 17. (a) Diagram of the deformation-based convertor (b) Diagram of the heavy plate.

3.2 Array System

Two potential devices naturally float on the surface of water without being anchored on the river/lake floor to harness the random, slow and low frequency oscillatory wave energy. Obviously, the power output of one single convertor is insignificant. To increase the overall power output, each single device is connected to each other by bus as a network system shown in Fig.18. In this case, every convertor can work together to produce electricity. The system looks like the fishing net floating on the surface of the water and anchored on the land. As the waves move forward and return periodically, each convertor harnesses the wave energy individually, and the bus will gather the electrical power to a terminal. The power generation of such system depends on the number/density of the devices connected electrically.

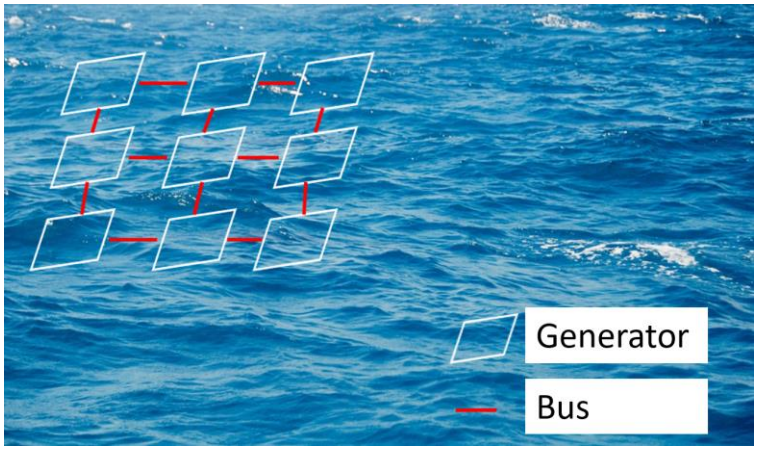

Figure 18. Schematic illustration of the network system.

CHAPTER 4

Physics of the Piezoelectricity

Piezoelectricity is the generation of electric charge when material is subjected to mechanical stress or deformation. When a piezoelectrical material is stressed, its atomic structure changes causing the formation of a dipole moment, which results in a voltage difference across the material. This is called the direct piezoelectric effect, first discovered by Curie in 1880 (Short history of piezoelectricity, n.d.). A dipole moment μ forms when two oppositely electrically charged particles of charge q are separated by a distance d. It is equal to $\mu = qd$. A piezoelectric material comprises of quartz (SiO_2) sandwiched between two metal sheets, which has a positive charge on one side and a negative charge on the opposite side when it is deformed. Fig. 19 illustrates the piezoelectricity effect. Before having any deformation, the piezoelectric crystal contains exactly balanced charges and there is no net charge on the surfaces. The load applied on the material forces the charges out of balance resulting in net positive and negative charges applied on both surface of the crystal, creating an electrical potential across the sides.

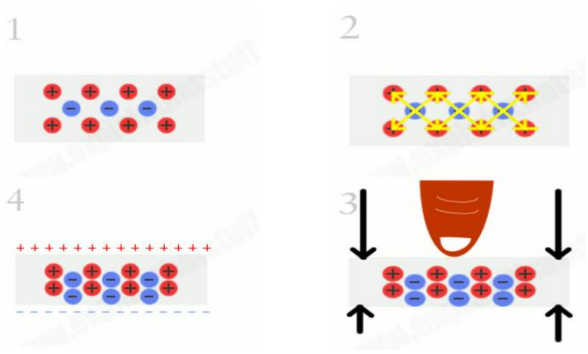

Figure 19. The process of piezoelectricity. (1) Charges are exactly balanced. (2) The effects of the charges exactly cancel out. (3) Applying force on the crystal. (4) Voltage appears across the opposite crystal surfaces (Woodford, 2017)

Two types of piezoelectric material have been commonly used, lead zirconate titanate (PZT) and polymer (PVDF). PZT has thick coating on metallic substrate, which allows it to be capable of withstanding relatively large strain. Usually, it is manufactured into the shape of rectangle or disk with high stiffness and it used as ultrasound transducers or actuators to convert mechanical energy into electricity. Unlike the PZT-based material, PVDF is more flexible and lightweight with high piezoelectric constant and low acoustic impedance. It has been used in various application such as automotive industry, medical and aerospace.

Figure 20. (a) Samples of the PZT (Standard quick-mount bending generator, n.d.) and (b) Samples of the PVDF (Small PVDF piezo film tabs, n.d.)

CHAPTER 5

Theoretical Simulation and Results

This chapter explains theoretical modeling of the wave converters and presents details of ANSYS and numerical simulations. The fluid interaction is coupled with equivalent mass-spring-damper system for acceleration-based convertor and two bodies coupled system for deformation-based convertor. These models are used for optimization of the geometry of the two designs.

5.1 Acceleration-Based Convertor Simulation

5.1.1 Theoretical Model

A theoretical model has been developed to describe the dynamics of the acceleration-based generator and its potential to convert wave energy into mechanical energy. It is assumed that the travelling wave propagates along y and z axis, and it is normal to the walls of the convertor. The displacements caused by the wave can be described mathematically by harmonic functions

$$\Delta x = A_x \cos\left(\vec{k}.\vec{x} - \omega t\right) \quad \text{.....(6)}$$

$$\Delta z = \mathrm{A}_z \sin\left(\vec{k}.\vec{z} - \omega t\right) \quad \text{.....(7)}$$

In Eqs. (6) and (7), A_x and A_z are the amplitudes of the wave, $\vec{k}$ is the wave vector, ω is the angular frequency and t is the time. As a result of the wave motion, the undisturbed free surface will be displaced and the floating convertor will start to heave, which is presented in Fig. 21.

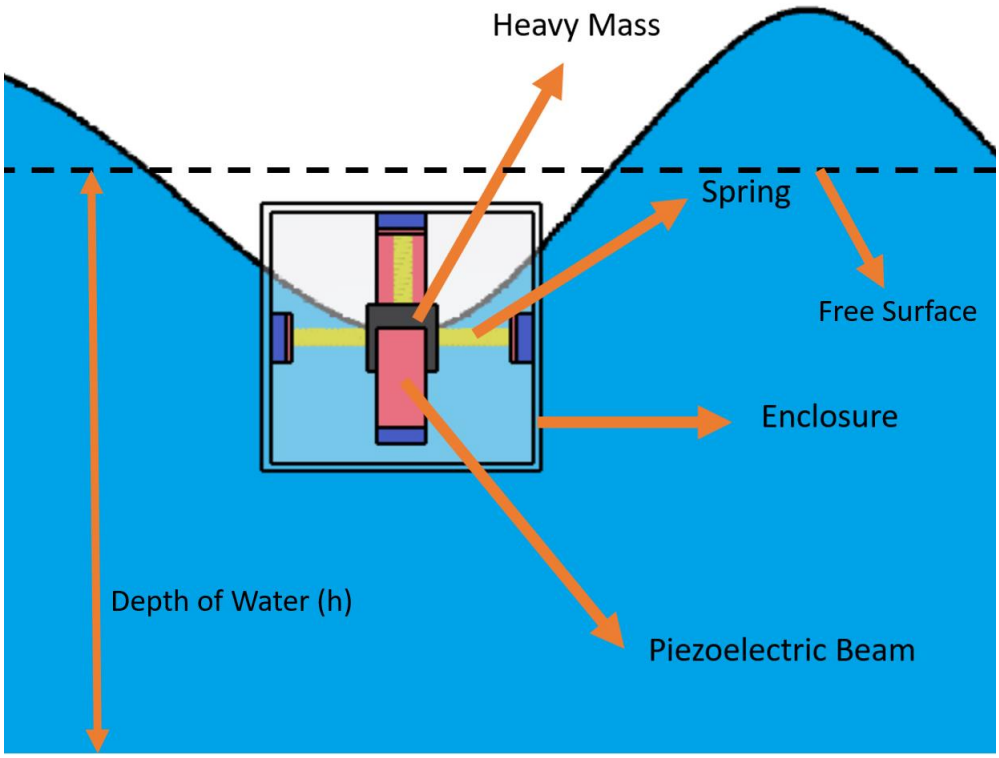

Figure 21. The convertor floats on the surface of water with travelling wave

This motion will result in reaction forces applied between the heavy mass and the enclosure. Fig. 22 shows the 3D free-body diagram including all forces acting on the convertor. In the vertical x direction, the enclosure is subjected to both gravity and buoyancy forces acting in the opposite directions. On the horizontal surfaces along y and z axis, the enclosure will be subjected to a drag force $\vec{F}_{\mathrm{d}}$

$$\vec{F}_d = \frac{1}{2} * C_d * \rho_w * (\vec{v}_w - \vec{v}_e)^2 * \frac{\vec{v}_w - \vec{v}_e}{|\vec{v}_w - \vec{v}_e|} \text{.....(8)}$$

In Eq. (8), ρ_w is the density of the water, C_d is the drag coefficient, $\vec{v}_w - \vec{v}_e$ is the relative velocity between the wave and the enclosure and $\frac{\vec{v}_w - \vec{v}_e}{|\vec{v}_w - \vec{v}_e|}$ determines the direction of the drag force. The velocity of the enclosure kept increasing until it reached the speed of the wave, given by the expression for the shallow water wave speed as follows (Hadzic, Hennig, Peric, & Xing-Kaeding, 2005)

$$\vec{v}_w = \frac{gA_x\vec{k}}{\omega} \times \frac{\cosh(\vec{k}\vec{y}+\vec{k}\vec{h})}{\cosh(\vec{k}\vec{h})} \times \cos(\vec{k}\vec{x} - \omega t) \ldots\ldots\ldots\ldots\ldots\ldots\ldots\ldots (9)$$

where h represents the depth of the water.

The resultant forces (F_r) are applied on the spring connections, which acts on both the inertia mass and the enclosure driving vibrations of the tip of the piezoelectric beam. The power take-off force (F_{PTO}) is accounting for the damping of the portion of the mechanical energy to electricity by the piezoelectric generators.

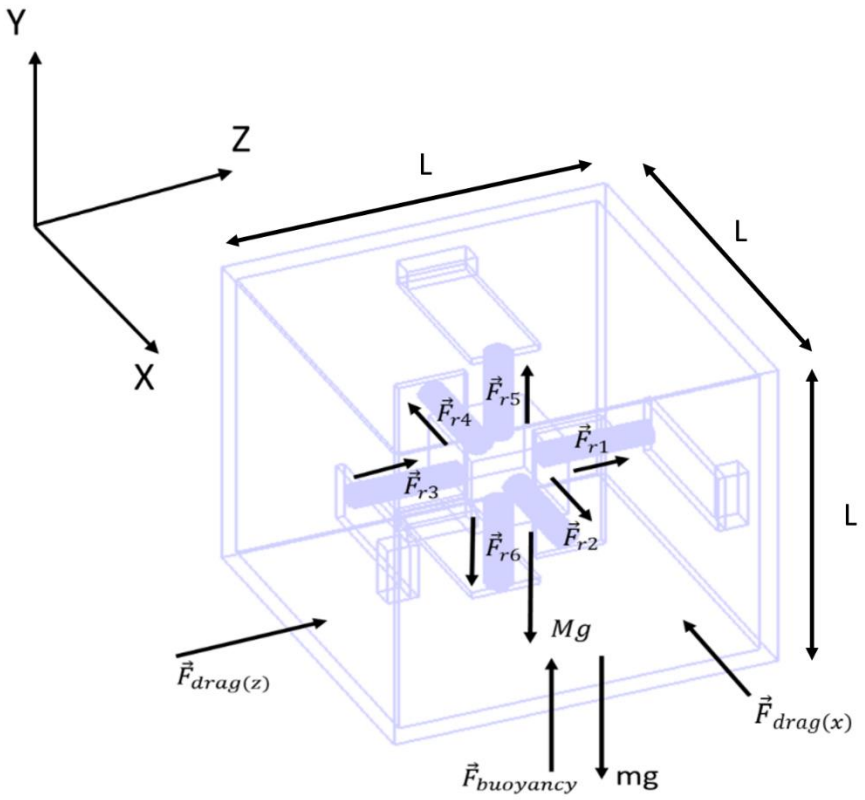

Figure 22. 3D model of the equivalent mass-spring-damper system.

Given that x is the vertical axis, the motion for the coupled mass-spring-damper system is given by the following system of equations

$$M\frac{d^2\vec{X}}{dt^2} = \sum_{r=1}^{6}\vec{F}_{rx} - Mg - \vec{F}_{PTOx} \ldots\ldots\ldots\ldots\ldots\ldots\ldots\ldots (10)$$

$$M\frac{d^2\vec{Y}}{dt^2} = \sum_{r=1}^{6}\vec{F}_{ry} - \vec{F}_{PTOy} \quad \text{.....(11)}$$

$$M\frac{d^2\vec{Z}}{dt^2} = \sum_{r=1}^{6}\vec{F}_{rz} - \vec{F}_{PTOz} \quad \text{.....(12)}$$

$$m\frac{d^2\vec{X}}{dt^2} = \vec{F}_b - mg + \sum_{r=1}^{6}\vec{F}_{rx} \quad \text{.....(13)}$$

$$m\frac{d^2\vec{Y}}{dt^2} = -\vec{F}_{d(y)} + \sum_{r=1}^{6}\vec{F}_{ry} \quad \text{.....(14)}$$

$$m\frac{d^2\vec{Z}}{dt^2} = -\vec{F}_{d(z)} + \sum_{r=1}^{6}\vec{F}_{rz} \quad \text{.....(15)}$$

Eqs. 12 - 17, can be solved numerically to obtain information for convertor displacements and velocity as a function of time.

5.1.2 ANSYS Harmonic Response Model

Based on the mathematical model described in the previous section, ANSYS 14.5 was used to estimate the feasibility of the proposed energy convertor. In ANSYS, a harmonic response model was used to simulate the motion of the wave convertor. Harmonic analysis determined the response of the structure of the convertor under steady state harmonic loading at a given single frequency. The converter was expected to be a linear structure with steady-state response, and the harmonic response analysis could determine load and vibrations which vary harmonically with time. The modeled system was tested for a wave environment with 0.1 – 1 Hz wave frequencies and 0.1 – 10 cm wave amplitudes, respectively, by assuming the converter only had vertical motion when it was subjected into water wave. The main purpose of the simulation was to obtain an estimate for the strain energy transferred to the piezoelectric generator at low frequency and small wave height, assuming that the strain energy would be transferred to electrical energy in high percentage. At the same time, the optimal generator size, mass ratio and spring stiffness were determined from these simulations. The initial setup was configured in such a way that the converter size was L = 15cm,

the mass ratio was 1 and the spring stiffness was 20 N/m. All the above parameters were optimized based on the frequency and amplitude of the target wave environment. The initial ANSYS simulation showed that the force on the piezoelectric generator was increasing with the wave frequency as shown in Fig. 23. The maximum load on a single piezoelectric beam calculated at the optimal conditions of wave with frequency of 1 Hz and amplitude of 10 cm was 3.9 N. By assuming that the strain energy of PZT beam could be transferred to electrical energy in high percentage, an estimate for the strain energy of a piezoelectric beam that could be converted to electricity could be obtained from

$$Strain\ energy = \frac{P^2 * {l_p}^3}{6 * E * I} \quad \text{.....(16)}$$

and the free body diagram of the PZT generator is presented in Fig. 24.

Using Eq. 16 (Budynas, 1998), with a known value of the force (P) and material properties of the PZT summarized in Table 2, the maximum strain energy that could be converted to electricity was found to be around 7.00±0.05mJ.

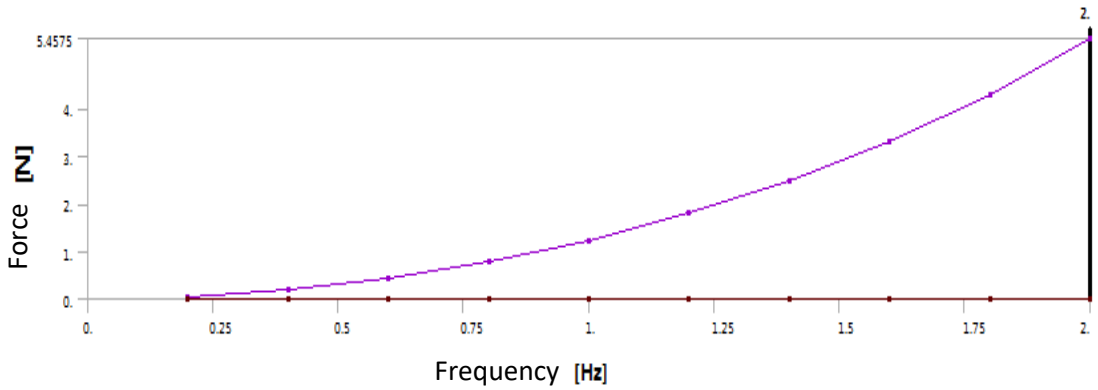

Figure 23. Force on the piezoelectric-generator as a function of wave frequency predicted with ANSYS.

Table 2. Material properties of PZT

Elastic modulus, E (Gpa)	Inertial mass, I ($kg.m^2$)	Width (mm)	Length (mm)	Thickness (mm)	Piezo charge constants (pC/N)	Piezoelectric voltage constants (10^{-3} Vm/N)
60	1.73×10^{-11}	0.0424	38.1	1.8	d33: 360 d31:-145	g33: 31.7 g31: -12.8

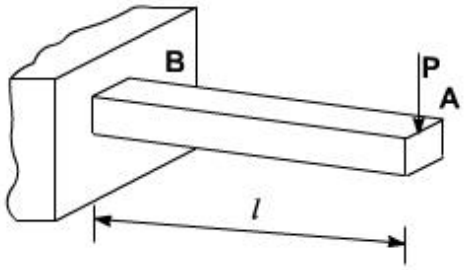

Figure 24Diagram of piezoelectric generator with a force applied on the tip (Sharma)

In order to achieve maximum power output, three factors – size of the convertor, inertia mass and the spring stiffness were further optimized. First, the size of the converter needed to be optimized, with controlled mass ratio and spring stiffness. In Fig. 25, the results from the simulations showed that the maximum power output of 8mW was attained at the size of the converter L = 10cm.

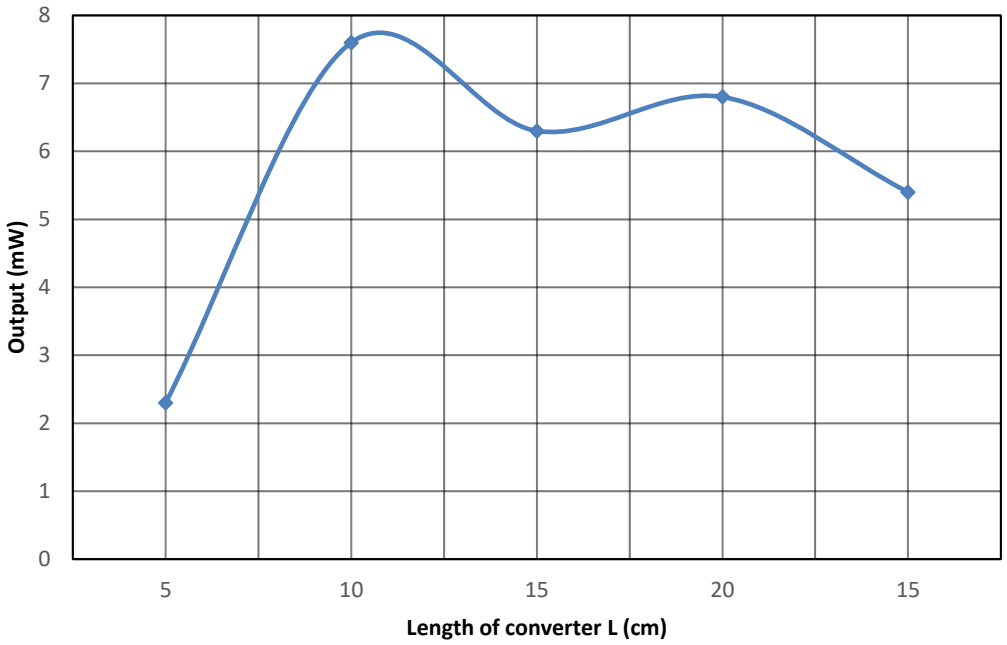

Figure 25. Optimization of the convertor length as a function of the energy output.

Fig. 26 represents the results from optimization of the mass ratio (m/M). The mass ratio was defined as the mass of the enclosure divided by the inertia mass. Both displacement and strain energy rose with the increasing mass ratio. Since the displacement of the inertia mass was limited by the size of the enclosure, the optimal mass ratio would be the one that corresponds to the maximum displacement allowed by the system. The vertical line in Fig.26 indicates the optimal mass ratio to be 0.65.

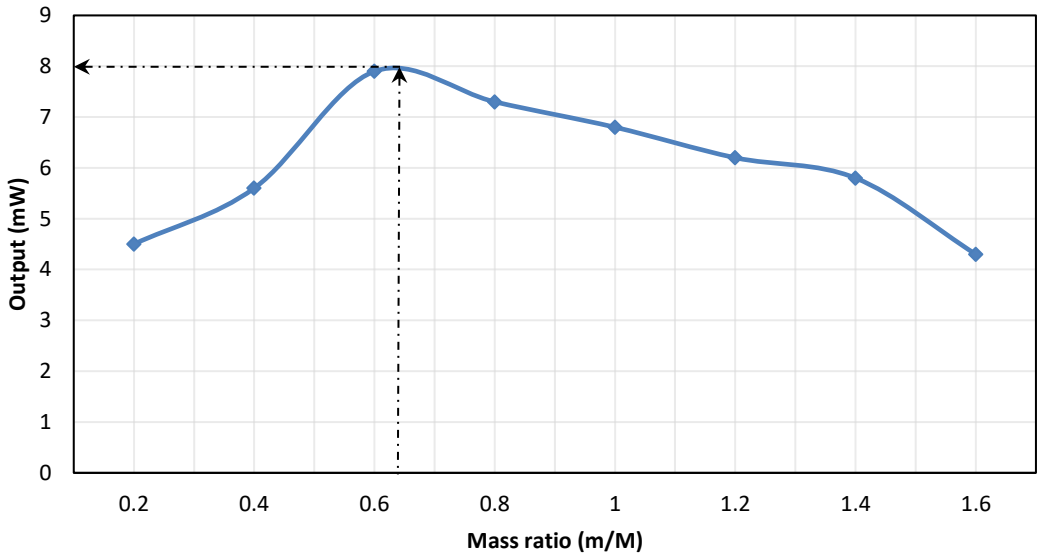

Figure 26. Optimization of the mass ratio as function of the convertor output power.

It indicates that the inertia mass, M, should be much heavier than the box, m, so that the strain energy reaches maximum under the wave action. Next step was to optimize the stiffness of the springs connecting the inertia mass with the piezoelectric generators. The maximum strain energy conversion theoretically could be achieved at spring stiffness corresponding to resonance frequency of 1Hz. However, due to the displacement constrains, the maximum extractable strain energy was ~10mJ, and it was achieved at spring stiffness of 10 N/m as shown in Fig. 27.

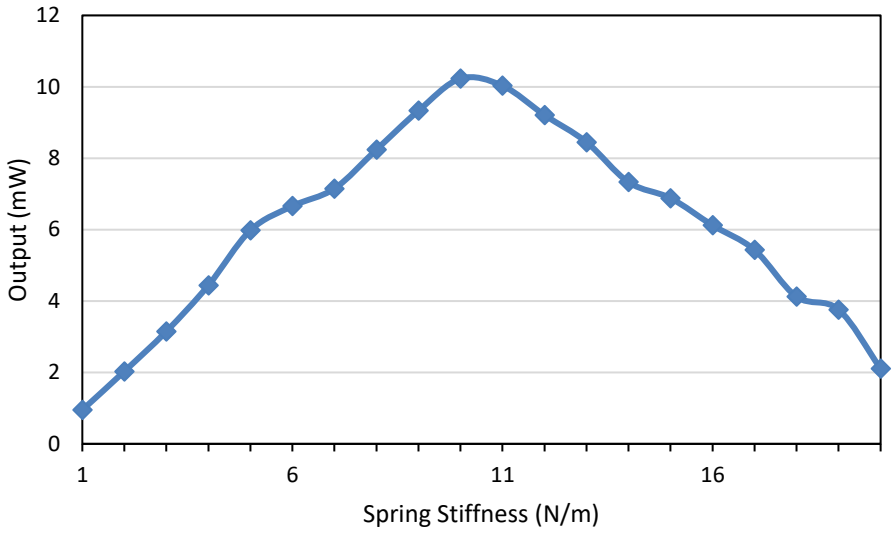

Figure 27. Optimizing the spring stiffness for a single piezoelectric beam as a function of the output power.

For the optimal convertor size of 10cm, mass ratio of 0.65 and spring stiffness of 10N/m, it was predicted that a single convertor consisting of 6 piezoelectric generators could produce ~ 10.00±0.05mJ energy per wave period of 1 seconds (at 1Hz wave frequency), which corresponded to ~10.00±0.05mW output power.

5.1.3 Numerical Simulation

To account for the real action of the wave, the governing equations (Eqs. 10 - 15) describing the convertor motion were solved numerically. The system of ordinary differential equations (ODEs) exhibited "stiff" behavior, which was resolved with the use of the GEAR method for implicit integration of ODEs. The wave conditions that were used in the simulations included waves with frequencies in the range of 0.2 – 1 Hz, amplitudes between 0.2cm and 10cm and the density of the water was 1000kg/m^3. With the help the numerical simulation, two important parameters - mass ratio and size of the enclosure would be determined, which were going to be compared with the results from the ANSYS simulation. Fig. 28 presents the initial position of the converter

in three different planes as the wave impacts the converter. In the (x-y) plane, the wave was coming from y direction, which forced the light enclosure to have a forward motion. However, the heavy inertia continued at rest and the oscillations of the springs were delayed so that there was a relative displacement between the heavy mass and enclosure. At the same time, the spring connections had either compression or tension motion.

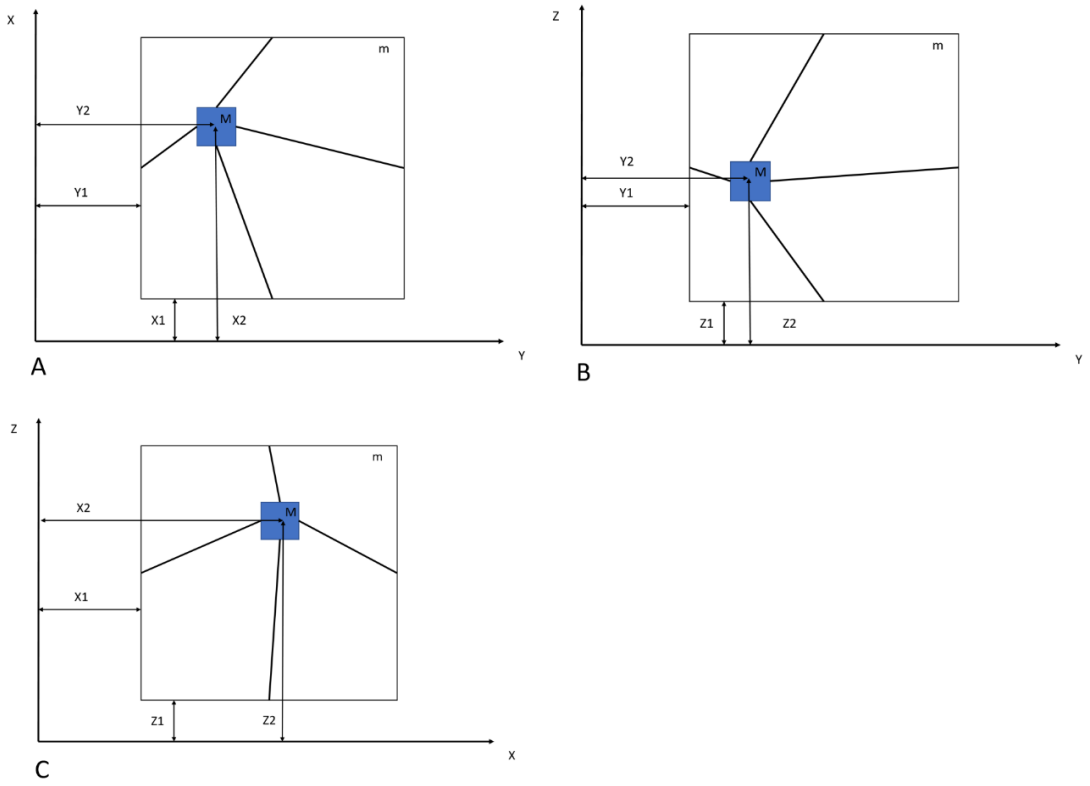

Figure 28. 2-D schematic diagram of design in three surfaces.

Since the buoyancy force was changing with the wave motion, the resultant force on the inertia mass/enclosure would continuously vary resulting in varied accelerations and relative displacement, so the strain energy of the springs would be constantly damping energy which was absorbed by the piezoelectric beams to generate electricity.

The resultant forces (F_r) existing in the spring connection followed the Hooke's law:

$$\mathrm{Fr} = -k_s * (l_c - l) \quad \text{.....(27)}$$

where k_s is the stiffness of the spring and equals to 10N/m, l is the natural length of the spring, and l_c is the length of the spring after compression and tension. The MATLAB code with the components of the forces acting at each surface can be found in the Appendix A. So far, the resultant forces had been determined and the next step was to determine the damping energy of the spring, which could be assumed to be the mechanical energy that had been converted from wave motion. The F_{PTO} became

$$\vec{F}_{PTO} = C * \Delta\vec{v} \quad \text{.....(17)}$$

where C is the damping coefficient and Δv presents the velocity difference between the wave and the convertor. The average damping coefficient was 20 N.s/m when the frequency was varying from 0.1Hz to 1Hz for the stainless-steel spring connections. By integrating the "dumping" force the actual harvested energy could be obtained as

$$E_d = \int C * \Delta v \, dt \quad \text{.....(18)}$$

The power take-off from the spring was achieved which equaled to the strain energy converted to the electrical power.

It should be noted that the accelerations of the inertia mass (M) and the enclosure (m) were different, causing the relative displacement between them presented in Fig. 29. Both objects experienced a sudden movement along with high frequency and irregular oscillations. In the first two seconds, the maximum relative displacement reached 0.6cm due to the instantaneous acceleration. Gradually, the relative displacement tended to be periodic and regular in a range of ± 0.1cm.

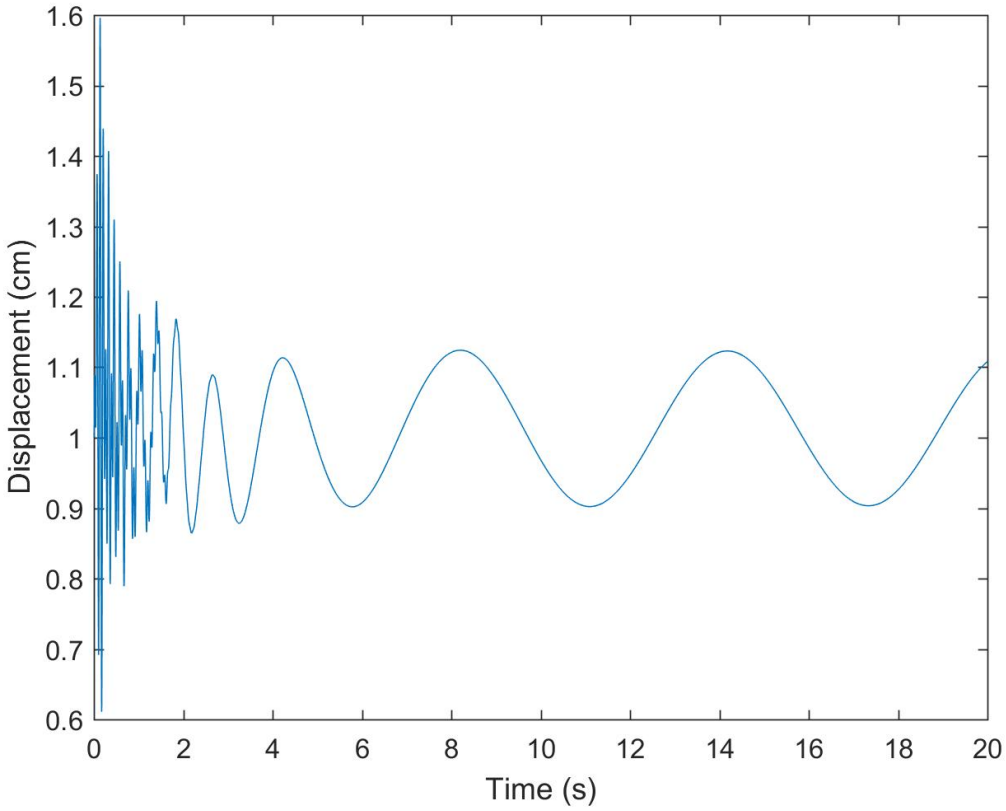

Figure 29. Relative displacement of heavy mass and enclosure

The convertor's power output strongly depended on the mass ratio between the enclosure and the heavy inertia (m/M). Fig. 30 shows the predicted power output as a function of the mass ratio m/M at different conditions.

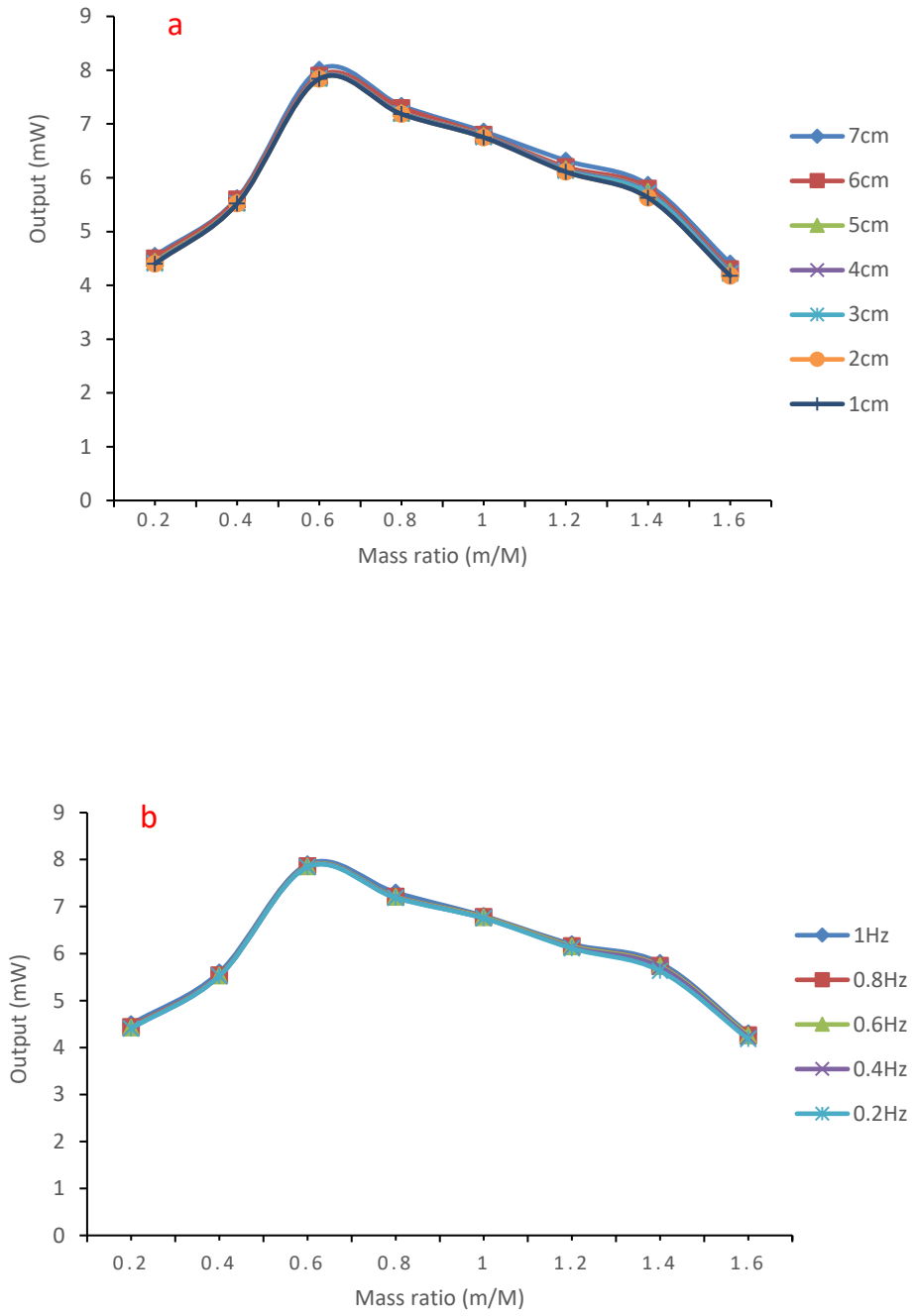

Figure. 30 (a) Power output vs mass ratio at different wave frequencies; (b) Power output vs mass ratio at different wave amplitudes.

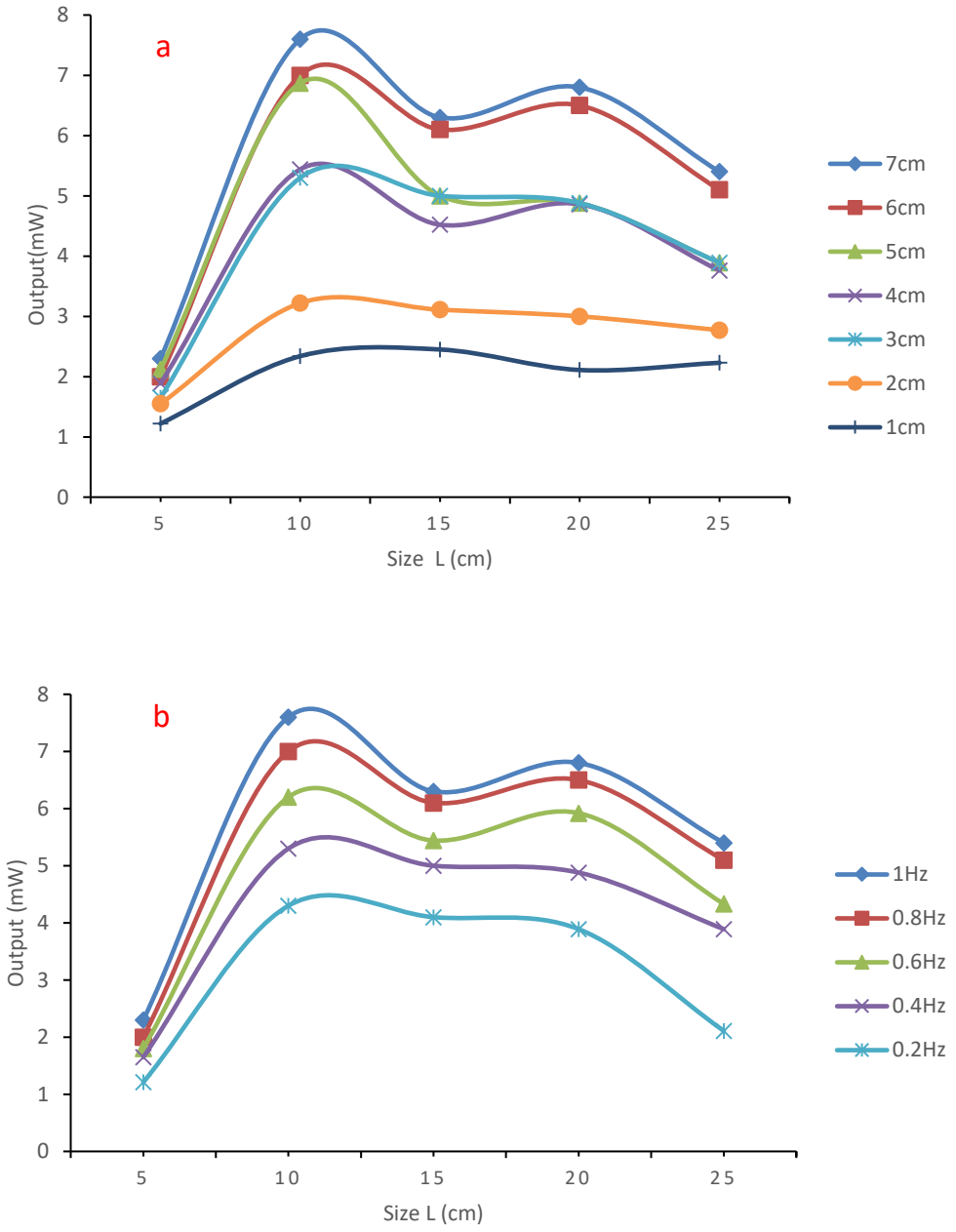

Figure 31. (a) Power output vs convertor size at varying wave frequency (b) Power output vs side length at varying wave amplitude.

Clearly, maximum power output was achieved at an optimal mass ratio of m/M ≈ 0.65. The magnitude of the optimal mass ratio was practically independent of the wave frequency and amplitude (Figs. 30a and 30b). The size of the convertor was the other important parameter for power output since it determined the magnitude of the

acceleration and displacement of the device. Fig. 31 shows the performance of different size convertors at different wave conditions. The power generated was strongly influenced by the wave's frequency and amplitude. In Fig. 31a, the output was affected by the wave amplitude, where all the curves had similar shape and reached the maximum value when the size of the convert was L = 10cm. Fig. 31b shows the same situation as Fig. 31a, and the maximum output obtained when the frequency was 1Hz and size of L = 10cm.

Comparing the results between harmonic response model and numerical simulation, it was clear that the optimal size of convertor and mass ration were similar for both simulations. The optimal mass ratio is independent of the wave environment, and has a constant optimal value of 0.65(Fig.30). There is also an optimal converter size with an optimal value of L ~10cm, which is independent of the wave environment. Therefore, it can be concluded that the optimal power output design will be based on: stiffness of springs ~10N/m, size of convertor L = 10cm, and the mass ration (m/M) = 0.65. Based on these parameters, a prototype was built and field tested.

5.2 Deformation-Based Convertor Simulation

The deformation-based convertor is able to convert the wave energy into mechanical energy (deformation and strain). It takes advantage of the deformation experienced by a flexible body subjected to velocity gradients in a viscous fluid flow. The velocity gradients can be created by either waves or currents which will deform the flexible piezoelectric (PVDF) material to generate electrical energy.

5.2.1 Preliminary Design

A preliminary prototype was designed to optimize the geometry of the deformation-based convertor. The two initial designs, A and B, are depicted in Figs. 33

and 34. While Design A had the piezoelectric polymer wrapped around the edges of the plate, Design B had only strips of polymer attached to the sides of the plate. The premise for Design A was to test the hypothesis that the water wave motion will create a traveling deformation wave throughout the whole polymer sheet regardless of the direction of the incident wave. For Design B, all polymeric strips were attached to the plate and they move independently. Once the wave propagated, each strip would be deformed due to the wave motion and wave impact. For the preliminary tests, vinyl was selected as a substitute material for piezoelectric polymer (PVDF) due the close similarity of the mechanical properties of both materials listed in Table 3.

Table 3. Material properties for Design A and B.

Vinyl Density (g/cm^3)	Tensile Strength (MPa)	Tensile Modulus (GPa)	Acrylic Density (g/cm^3)
1.78	50	1.7	1.18

The two designs were tested in the laboratory flume shown in Fig. 32, and the deformation of the vinyl sheets/strips was video recorded in order to assess the performance of the convertor and determine the maximum achieved deformation. During the experimental testing, the average flow velocity in the flume was kept at 2.87m/s while the total water depth was 160mm.

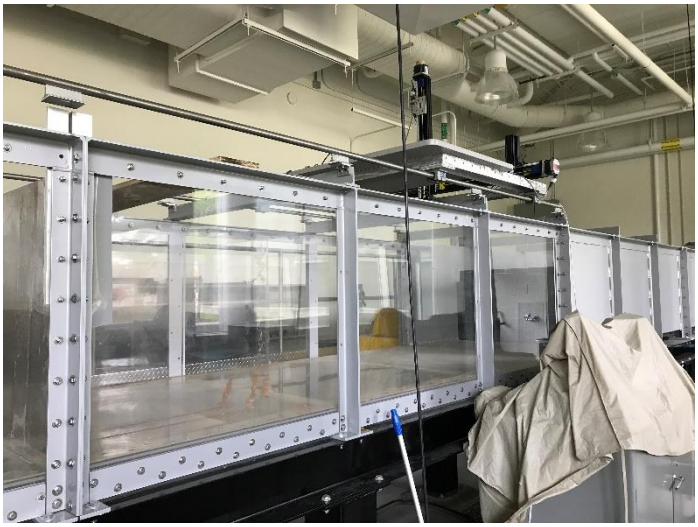

Figure 32. Flume setup

Fig. 33 shows two snapshots two views of the maximum deformation in Design A prototype. Clearly the polymer sheet wrapped around the plate had slight deflection resulting in small deformation corresponding to small electrical output in the PVDF. In Fig.34, snapshot of the performance of the Design B prototype is shown. The strips had significant deflection/deformation significantly exceeding the deformation in Design A. Therefore, Design B concept was adopted for the final design of the deformation-based convertor.

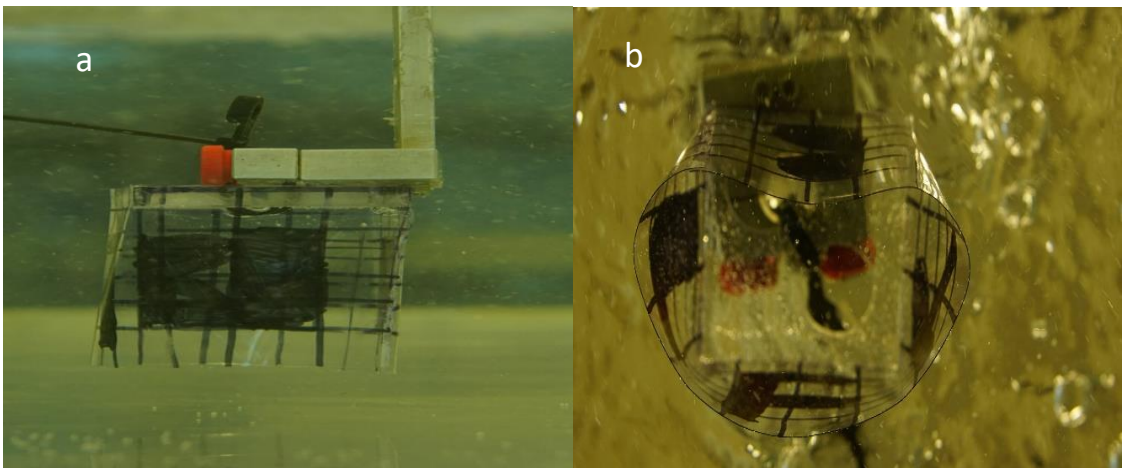

Figure 33. (a) ‘Design A’ side view; (b) ‘Design A’ bottom view

Figure 34. ‘Design B’ side view

Since the adopted Design B has multiple flexible strips resembling jellyfish tentacles, we’ll refer to this design as “jellyfish”. A variation of the “jellyfish” design –the “reverse jellyfish” was also experimentally tested. While the in “jellyfish” convertor the flexible strips were underneath the floating plate pointing downwards, in the “reverse jellyfish” the flexible strips were pointed upwards from the completely submerged heavy plate. The buoyancy needed for keeping the convertor on the surface was provided by the small buoys of foam attached to the tips the piezo polymeric strips shown in Fig. 35.

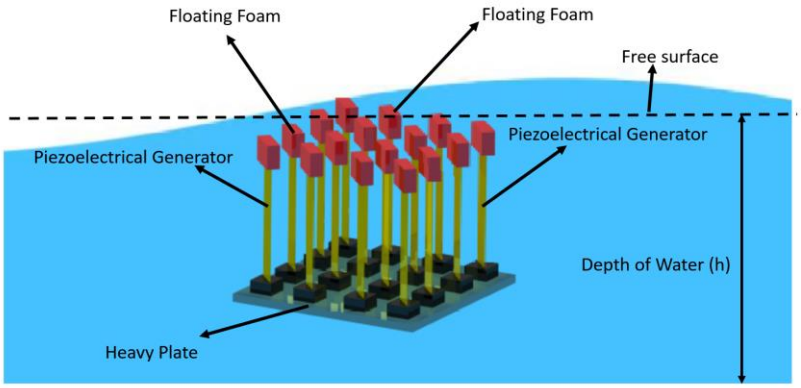

Figure 35. Schematic diagram of the reverse jellyfish generator

Both concepts – “jellyfish” and “reverse jellyfish” convertors were tested in wave environment with wave speed of 0.3m/s, wave frequency of 1Hz and the variable wave amplitude - 2 to 5cm. The total power output was recorded and the results are shown in Figure 36. While, the power output for both convertors are increasing with the increase of the wave amplitude, the ‘reverse jellyfish’ convertor showed significantly higher power output.

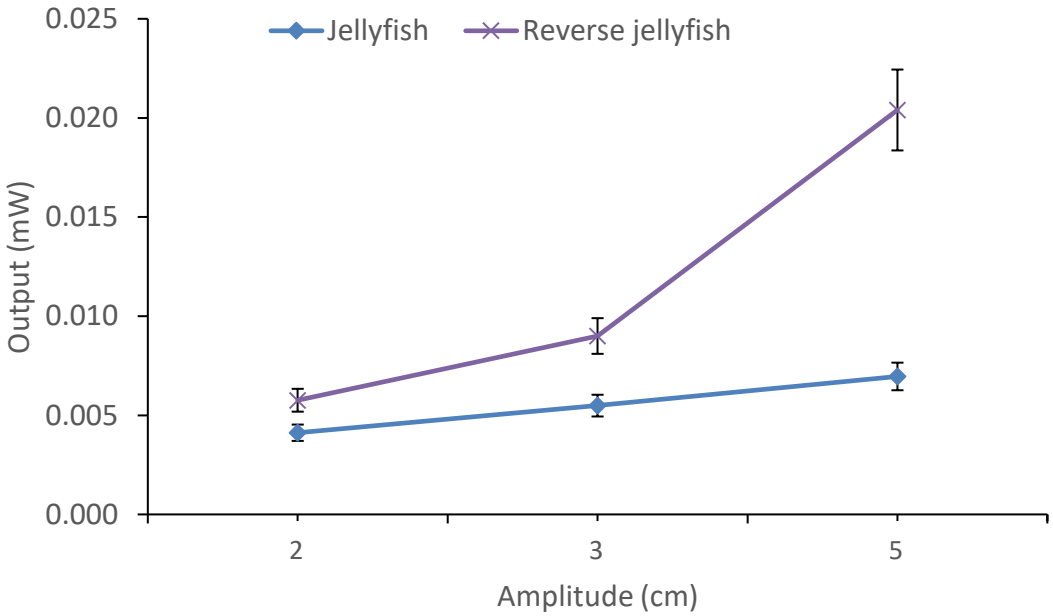

Figure 36. Output comparison between two concepts at 1Hz.

The reverse jellyfish design was taking advantage not only of the wave motion but also of the current flow. The heaving of the floating buoys contributed to the oscillatory motion of the convertor. On the other hand, the water current passed through the strips forcing them to experience larger deformations. These effects enhanced the deformation of the strips providing for increase of the harvested electrical power.

5.2.2 Theoretical Model

A theoretical model was developed to describe the principle of operation of the deformation-based generator. Fig. 37 presents the 2-D free body diagram of the final "reverse jellyfish" design.

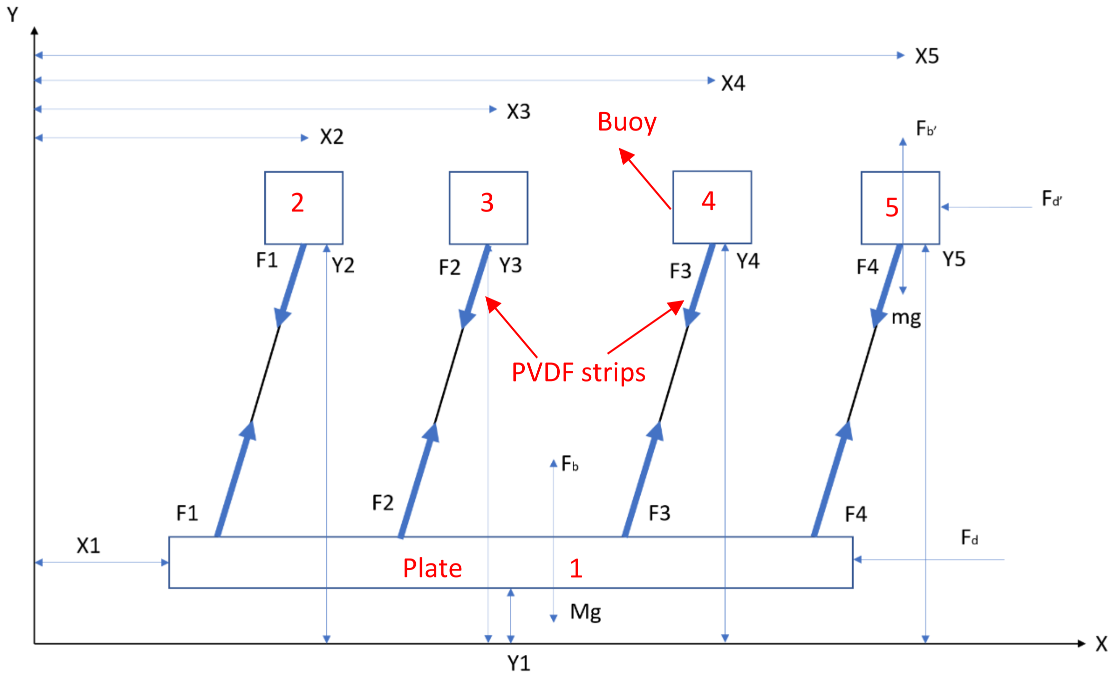

Figure 37. Free body diagram of the deformation-based convertor.

Let us assume that shallow wave is moving in the x direction and the expression for the wave displacement and wave speed given by (Hadzic, Hennig, Peric, & Xing-Kaeding, 2005)

$$\Delta x = A * \cos(ky - \omega t) \quad \ldots\ldots\ldots\ldots\ldots\ldots\ldots\ldots\ldots\ldots (19)$$

$$V_{wave} = \frac{gAk}{\omega} \times \frac{\cosh(kx+kh)}{\cosh(kh)} \times \cos(kx - \omega t) \quad \ldots\ldots\ldots\ldots\ldots\ldots (20)$$

In Eqs. 19 and 20, k is the wave constant, ω is the angular frequency, A is the wave amplitude, t is the time and h is the depth of the water.

Under the action of the wave, the buoy will start not only to heave under the wave displacement but they will be translated forward, in the streamwise direction. The equations of motion of the buoy are as follows.

$$\frac{d^2y_i}{dt^2}m_f = -gm_f + F_b^b - F_{y,i-1}; \quad i = 2,3,4,5 \ldots\ldots\ldots\ldots\ldots\ldots (21)$$

$$\frac{d^2x_i}{dt^2}m_f = -F_d^b - F_{x,i-1}; \qquad i = 2,3,4,5 \ldots\ldots\ldots\ldots\ldots\ldots (22)$$

where m_f represents the mass of the floating buoy, F_b^b is the buoyant force, F_{yi} are the tension/compression forces applied on the PVDF strips along the y axis, F_d^b is the drag forces of the foam and F_{xi} are the tension/compression forces applied on the PVDF strips along the x. The buoyancy force, F_b^b , varies depending on the submerged volume of the buoy.

$$F_b^b = \rho_w g V_b \ldots\ldots\ldots\ldots\ldots\ldots\ldots\ldots\ldots\ldots\ldots\ldots\ldots\ldots\ldots\ldots\ldots\ldots (23)$$

where ρ_w is the density of water and V_b is the submerged volume of the buoy.

The drag force is given by

$$F_d^b = -\frac{1}{2} * \rho_w * C_d * \Delta v_b{}^2 * A_b * sign(\Delta v_b) \ldots\ldots\ldots\ldots\ldots\ldots\ldots\ldots\ldots\ldots (24)$$

where ρ_w is the density of water, C_d is the drag coefficient, Δv is the velocity difference between the wave and the buoy and A_b is the cross-sectional area.

The equations of motion of the fully submerged plate are as follows,

$$\frac{d^2y_1}{dt^2} * M_P = -M_P g + F_b^P + \sum F_{y,i-1}; \quad i = 1,2,3,4 \ldots\ldots\ldots\ldots\ldots\ldots (25)$$

$$\frac{d^2x_1}{dt^2} * M_P = -F_d^P + \sum F_{x,i-1}; \qquad i = 1,2,3,4 \ldots\ldots\ldots\ldots\ldots\ldots (26)$$

In Eqs. 25 and 26, M_p is the mass of the plate, F_b^P is the buoyant force, $\sum F_{y,i-1}$ presents the overall reaction forces in the PVDF strips in the y direction, F_d^P is the drag force, $\sum F_{x,i-1}$ represent the overall reaction forces in the strips along the x direction. The drag force varies with the relative velocity between the plate and water flow.

$$F_d^P = -\frac{1}{2} * \rho_w * C_d * \Delta v_p{}^2 * A_p * sign(\Delta v_p) \ldots\ldots\ldots\ldots\ldots\ldots\ldots\ldots\ldots\ldots (27)$$

where ρ_w is the density of the water, C_d is the drag coefficient, Δv_p is the velocity difference between the wave and plate and A_P is cross-section area of the plate.

In the coupled system, plate - floating foam, the relative motion is initiated by the wave motion and the velocity gradient in the flow (Fig. 38). This relative motion results in the deformation/deflection of the connecting PVDF strips which in turn is converted into electrical energy.

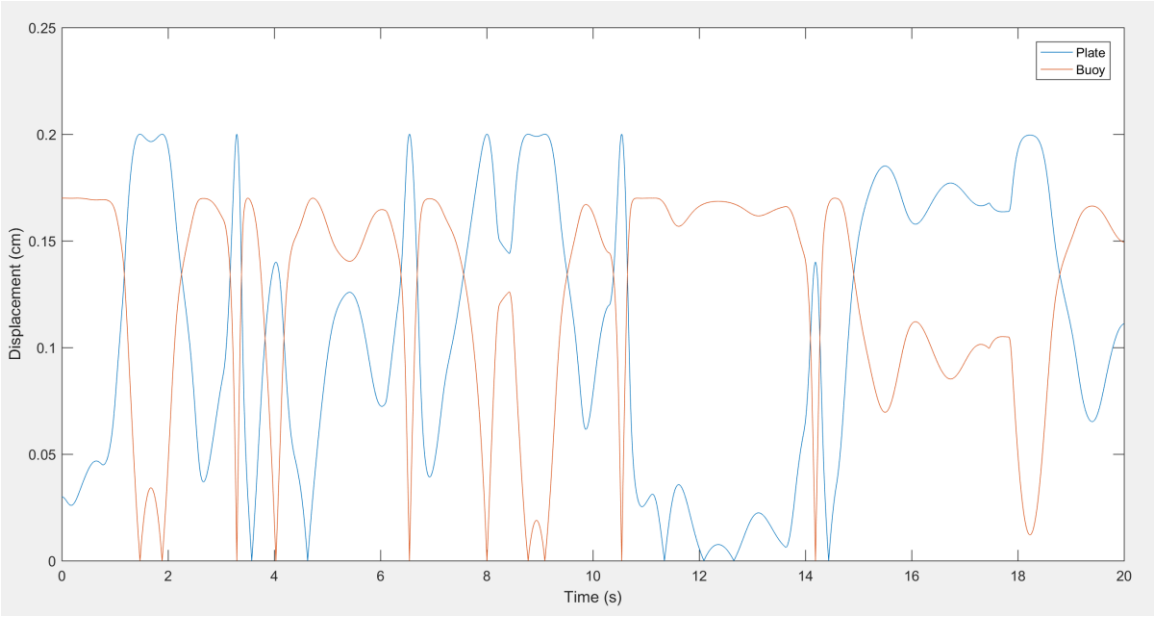

Figure 38. Displacements of the plate and floating foam.

5.2.3 Numerical Simulation

Solving the "multi-body problem" of the several bodies coupled system constitutes a significant numerical challenge. The proposed convertor which consists of 16 piezo strips and a plate was divided into 16 two-bodies systems. Eqs. 21, 22, 25 and 26 describing the motion of each of the two-body systems were solved numerically. The target wave environment included waves with frequencies in the range of 0.2 Hz – 1 Hz and amplitudes between 0.2cm and 7cm. The size of the floating buoy was selected to provide enough buoyancy so that the entire system is floating. The reaction forces exerted on the PVDF strips were determined from the geometrical constraint of a constant length of the strips. The components of the reaction forces are included in Appendix C. The governing equations constitute a system of ordinary differential equations with algebraic constraints, which is solved with variable backward differentiation formulas (BDFs) of orders 1 to 5 used with index-1 differential algebraic equations (DAEs) solver (MATLAB ode15i). The consistent initial conditions for this first-order implicit DAEs system was determined by the 'decic' MATLAB function. Next step was to find the electric power generated by the PVDF strips.

5.2.4 Energy Harvesting

The PVDF strips consists of three polymer layers in total with protective coating, piezo film and polyester laminate respectively. The piezo film plays the essential role as it converts the bending motion into electric power output. The structure of the PVDF strips is presented in Fig 39.

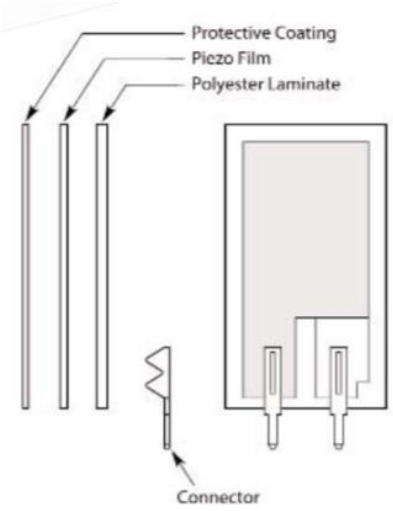

Figure 39. Three layers of the PVDF structure (Piezo film product guide and price list)

The voltage across the film can be calculated as (Introduction to piezo transducers, n.d.),

$$V = \frac{3FL_P g_{31}}{4WT} \quad \text{.....(29)}$$

where F is the load at the tip of the strip, L is the length of the film, W is the width, T is the thickness, and g_{31} is the piezoelectric constants. The dimensions and material properties of the piezo film are given in Table 4.

Table 4. Dimension and material properties of the PVDF strips (Piezo film product guide and price list)

Length (L_p) [mm]	Width (W) [mm]	Thickness (T) [mm]	Piezoelectric constant g_{31} $[\frac{V/m}{N/m^2}]$
170	18	0.205	216×10^{-3}

The overall energy output can be obtained using Eq. 29 and

$$P_p = \frac{1}{2} C_p V^2 / t \quad \text{.....(30)}$$

where $C_p$is the capacity of the film, V is the voltage of the film and t is the time.

Two sets of simulations were run to obtain the optimal dimension of the convertor. The overall power generated by the convertor was assumed to be the addition of the 16 power outputs of the two-body systems. First set of simulations was performed to optimize the size of the plate at various wave frequency and amplitude. Figs. 40 and 41 show the power output of the converter, at different frequencies (0.2Hz to 1.4Hz) and wave amplitude (1cm to 10cm). Each symbol in Figs. 40 and 41 represents one of the seven different convertor sizes.

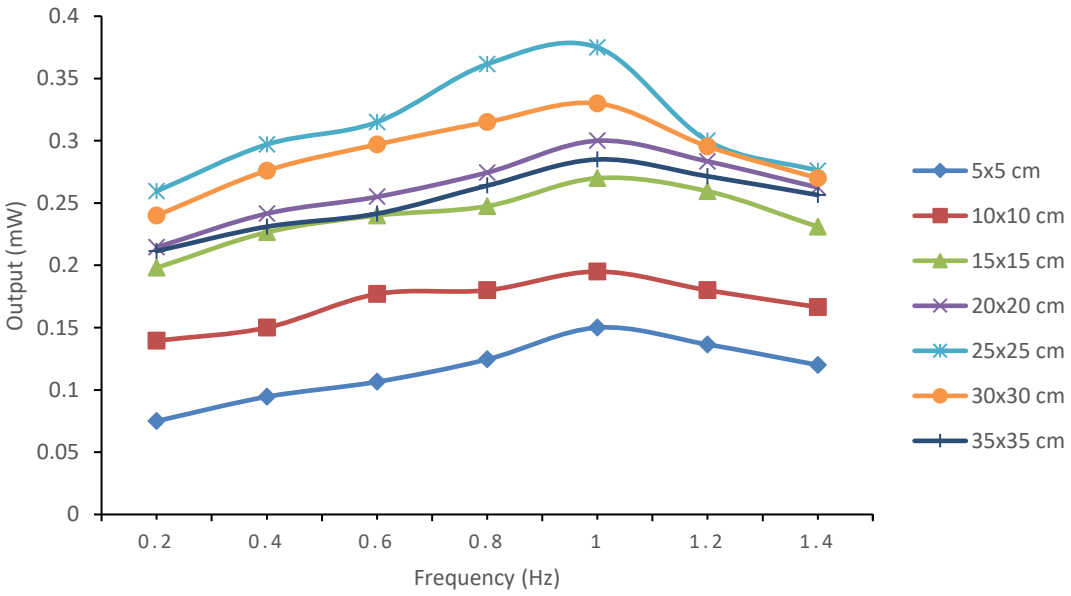

Figure 40. Performance of different convertor sizes at varying frequency.

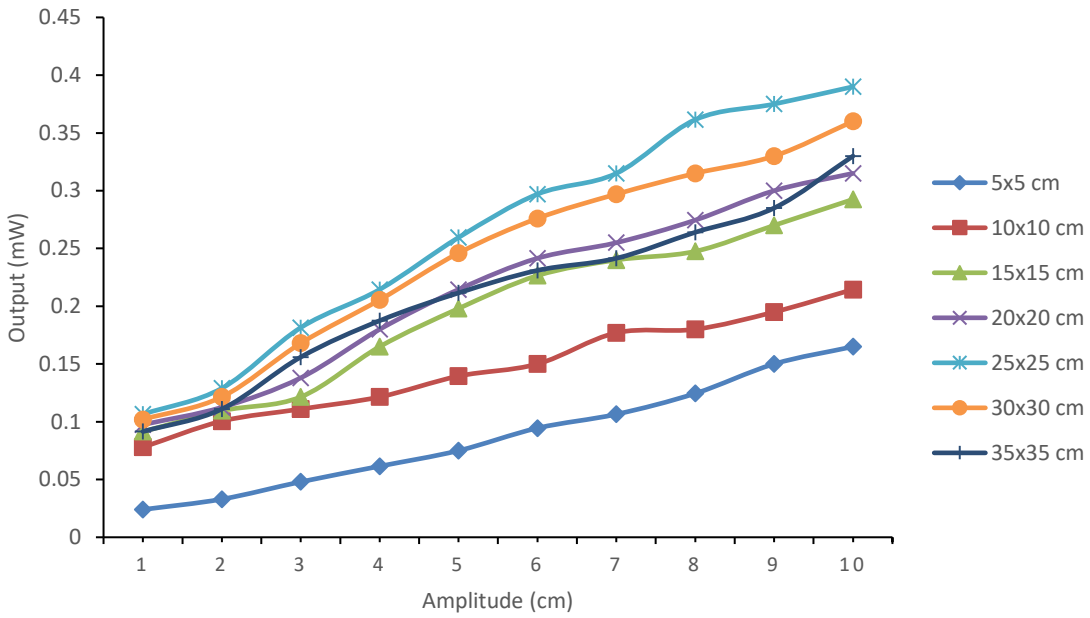

Figure 41. Performance of different convertor sizes at varying amplitude.

Fig. 40 indicates that different size converters reach the optimum power output at the same frequency ~ 1Hz, with convertor size equal to 25cm shows maximum power output with peak value of 0.37±0.0003mW. Fig. 41 shows monotonic increase of the output power for all convertors with the increase of the wave amplitude. Again, convertor with size L = 25cm showed the best performance among all convertors. Based on the two simulation tests a convertor with 25 × 25cm^2 plate was selected for further optimization. Next step was to determine the optimal length of the piezoelectric strips. Converters with 25 × 25cm^2 plate and different length strips was modeled at wave conditions of frequency of 0.2Hz – 1.4Hz and amplitude from 1 to 10cm. All curves in Fig. 42 showed optimal power output at ~1Hz with maximum power output of converted with stirp length of 20cm. The simulations performed at variable wave amplitudes (Fig.43) supported the conclusion that the maximum power output can be achieved at 20cm strip length. Due to the maximum deformation, the PVDF strips with 20cm length was selected as the optimal option.

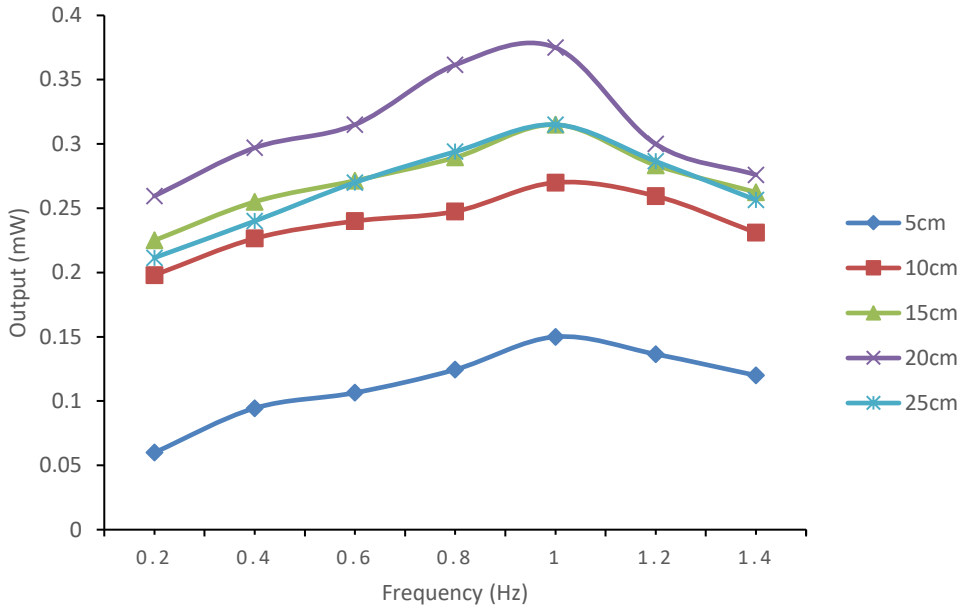

Figure 42. Performance test of different strips length for varying frequency

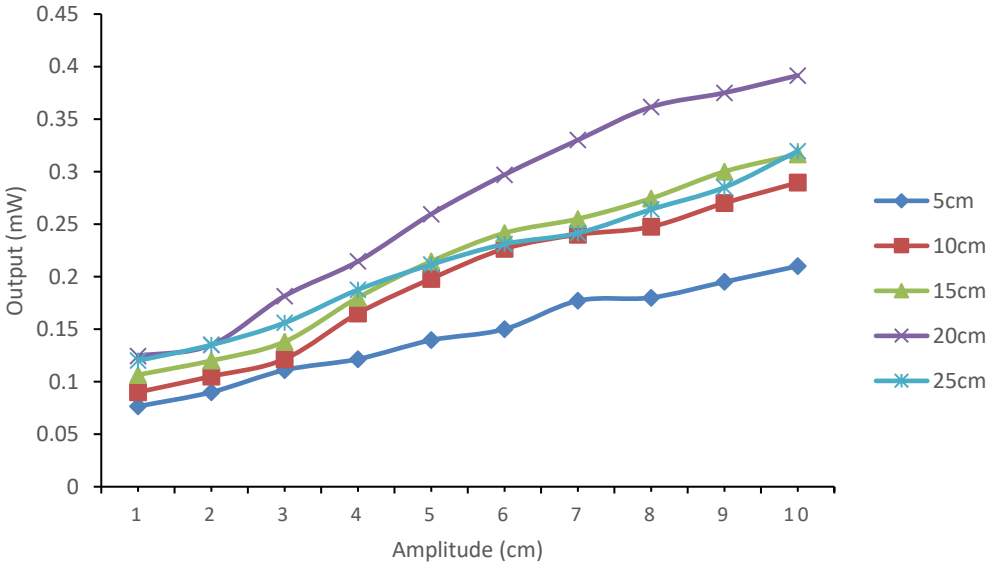

Figure 43. Performance test of different strips length for varying amplitude.

In conclusion, the deformation – based convertor with 25 × 25 cm^2 plate and 20 cm length strips is the optimal converter based on the numerical simulations. Number of prototypes were manufactured and further experiments are going to be conducted to test the functionality of the convertor.

CHAPTER 6

Experimental Result

In this chapter, the details of experiments for both convertor concepts are presented. It includes the field test result, the comparison between the experimental and theoretical results and the experimental results for the convertor array tests.

6.1 Field Experiment -Acceleration-based Convertor

After obtaining the theoretical simulation results, a prototype was built and tested at riverside with different wave environment conditions. The material of enclosure is a transparent acrylic plate, the heavy mass is made of stainless steel preventing corrosion and heavy enough to drive the piezoelectric beams. As it was mentioned in the previous chapter, the optimal size of the convertor is L = 10cm with mass ratio of 0.65 (m = 0.05kg, M = 0.132kg). The prototype was sealed, and the piezoelectric generators were connected to a DAQ terminal to record the power output of the convertor. In the field tests, the wave frequency detected was between 0.2 - 0.8Hz and the amplitude was 2 - 6cm.

Figure 44. Field test of the acceleration-based converter.

Unlike the numerical simulations, the wave conditions in the field test were not possible to control, since the wave frequency and amplitude depended on the weather at the time of the experiment. Four sets of field tests had been performed at different wave conditions which are listed in Table 5.

Table 5. Wave conditions of the field test.

Field Test	#1	#2	#3	#4
Amplitude(cm)	2	3	5	6
Frequency(Hz)	0.25	0.2	0.4	0.8

Fig. 45 represents the power output of a single convertor at the described wave conditions. In general, the power output grows as wave amplitude and frequency increases. The peak power output of ~5.0±0.6mW for the convertor was achieved at amplitude of 6cm and frequency of 0.8Hz. It was noticed that the output did not change significantly with the increase of the wave frequency from 0.2 to 0.4Hz and amplitude increase from 2 to 5cm. The output power jumped to the maximum value when the frequency reached 0.8Hz with a small amplitude increase from 5cm to 6cm. This points to the wave frequency as the dominant factor determining the power output of the converter.

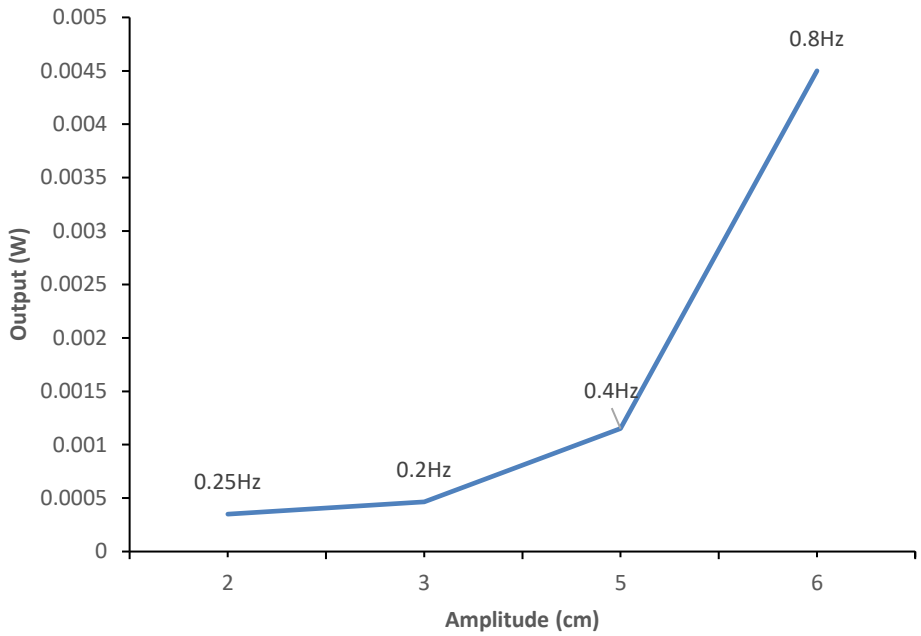

Figure 45. Power output - field test -Acceleration-based convertor

Fig. 46 shows the comparison between the theoretical simulation and the field tests results at the experimental wave conditions listed in Table 5. The theoretically predicted power output exceeded the experimentally obtained values. At small amplitudes (< 5cm), the difference between the theoretically predicted power output and the experimentally obtained was quite small. However, as the wave amplitude increased to 6cm (frequency of 0.8Hz), the prototype's power output was much lower than the simulation's one, with 31% error percentage This could be attributed to the energy losses in the spring connections and piezoelectric generators. In the numerical simulation, it was assumed that most of the strain energy of piezoelectric beams was transferred into electricity. The fact is that part of the strain energy was dissipated by the springs damping. Another reason was the wave conditions. The travelling wave set-up in the simulations was two dimensional with constant amplitude and frequency. In the field tests the actual wave conditions were more complex and volatile causing the lower output of prototype.

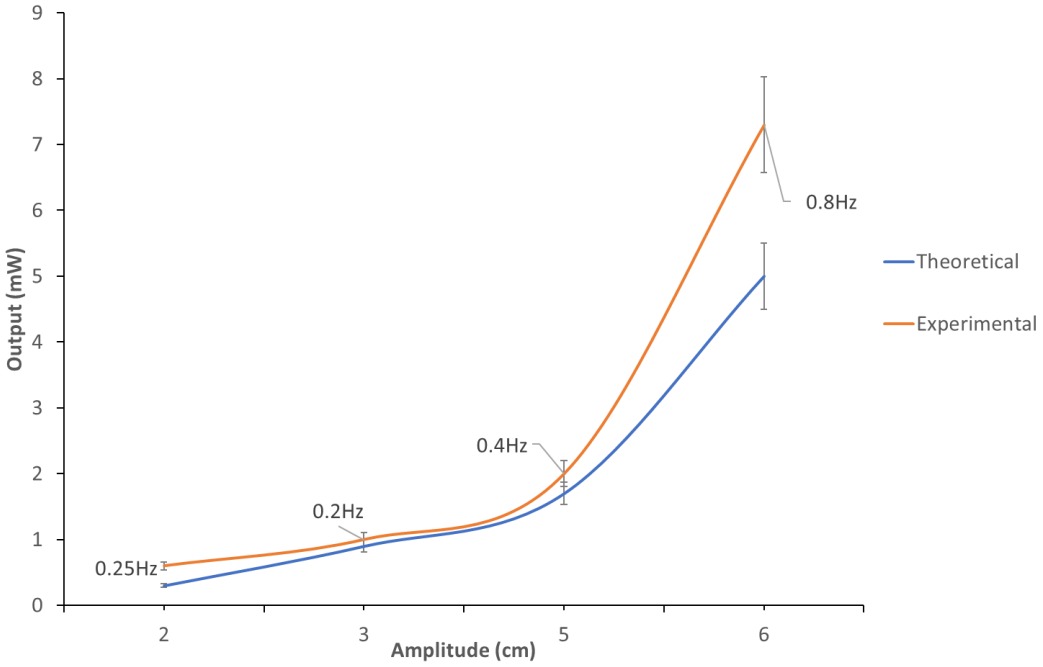

Figure 46. Output comparison between experimental and theoretical results.

6.2 Field Experiment -Deformation-based Convertor

The built prototype is shown in Fig.47. The inverse jellyfish plate was made of acrylic, and the piezoelectric strips were made of PVDF with 17cm length. The electrodes of the piezoelectric strips were protected by enclosing them in dielectric grease capsules.

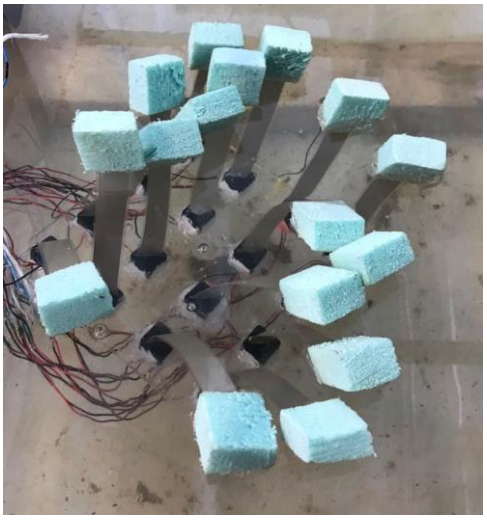

Figure 47. Prototype of the Deformation-based convertor.

The built prototype had 16 PVDF strips with overall mass of 2kg. The field testing was performed at several wave environment conditions as shown in Fig. 48. The PVDF generators were connected to a DAQ terminal, which recorded the power output of each PVDF strip of the converter. In the field tests, the wave frequency varied between 0.2 and 0.8Hz with wave amplitude between 2 and 7cm. Three sets of field tests were performed at wave conditions listed in Table.6.

Figure 48. Field test of Deformation-based convertor

Table 6. Wave conditions of the field test.

Field Test	#1	#2	#3
Amplitude(cm)	2	6	7
Frequency(Hz)	0.25	0.3	0.8

Fig.49 shows the power output of a single convertor at the target wave conditions. Clearly the power output of the converter monotonically increased as the frequency and the amplitude of the wave increased reaching a max value of maximum

value at 0.25±0.01mW (wave frequency of 0.8Hz and amplitude of 7cm). In the field testing the actual wave condition could not be controlled, since they depended on weather conditions at the moment of testing. Numerical simulations of the performance of the convertor at the field testing conditions were done and a comparison between these results are shown in Fig. 50.

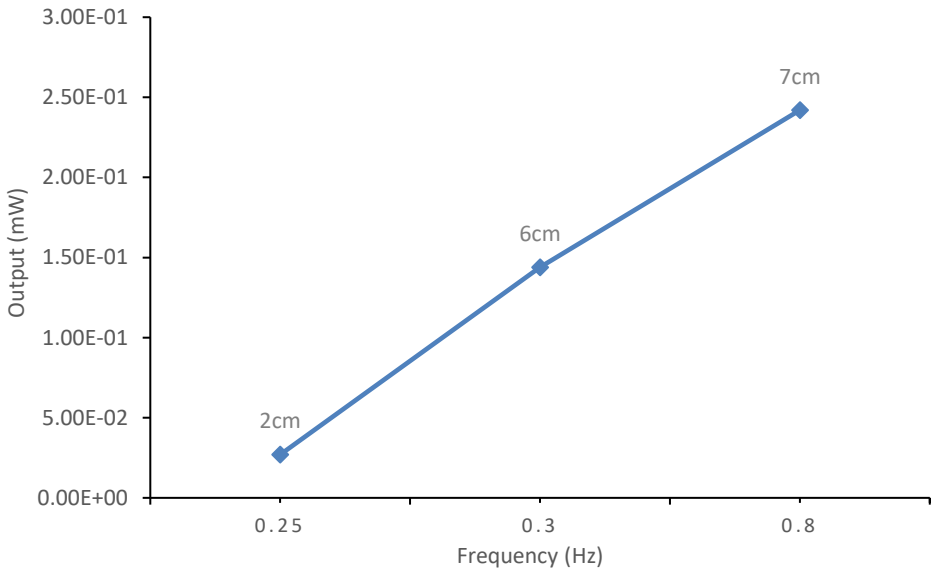

Figure 49. Power output - field test (Deformation-based convertor)

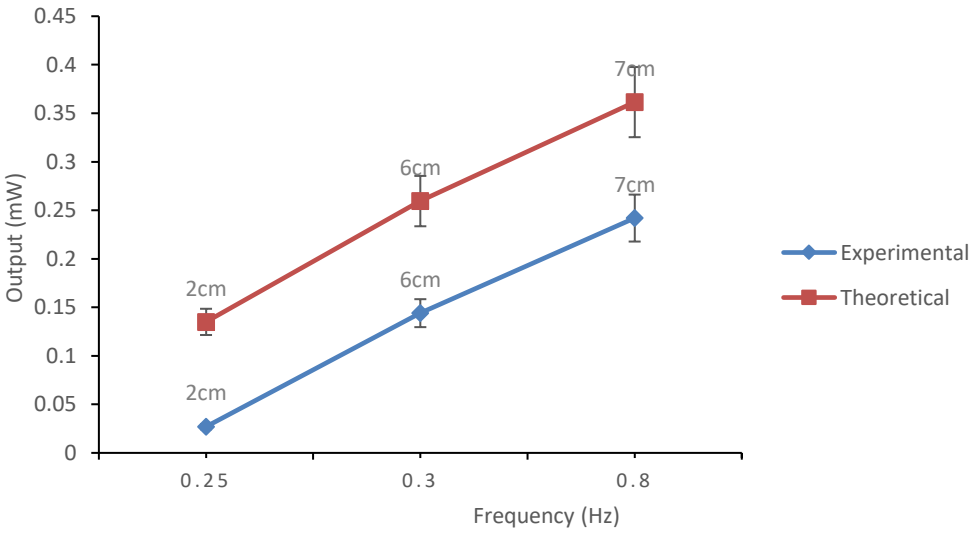

Figure. 50 Comparison between experimental and theoretical results.

The theoretically predicted power output of the convertor exceeds the experimentally obtained power output by ~ 33% percent. This is mainly due to the simplifications adopted in the developing of the model. Namely, replacing a coupled system of a plate and 16 piezoelectric strips with 16 two-body subsystems, restricting the interference between the individual piezoelectric strips. In addition, two extra factors, in the field test, contributed to the reduction of the converters power output. This factor is - aquatic plants wrapping around the strips and length of the mass of the DAQ connecting cable which influenced the motion of the whole system.

6.3 Array Test

To increase the overall power output of the wave energy convertors, an energy harvesting arrays were developed for each the two power generation concepts. A sketch of the such array/network of interconnected single devices, is shown in Fig. 18. The power generated of such network depends on the number/density of the devices and their mutual interactions/interference.

The array experimental testing was performed in laboratory conditions at controlled wave amplitude and frequency. The main goal of the experimental array testing was to find the optimal number of converters in the array along with the optimal position and inter convertor distances for maximum power output. Due to the power limitation of the wave maker and the size of the tank, the range of the reproduced wave conditions were restricted. During the array tests the wave frequency and the amplitude were maintained between 0 - 0.5 Hz and 0 - 3cm, respectively. In this case, the power output of a single converter was significantly smaller than the one obtained during the field tests.

6.3.1 Acceleration-based Array System

An array system for acceleration-based convertor was built as a 3 × 2 array as shown in Fig. 51, and tested in controlled wave conditions. The positions of the convertors in the array were varied, while the distance between the units was also adjusted from 5cm to 25cm in order to determine the optimal array configuration.

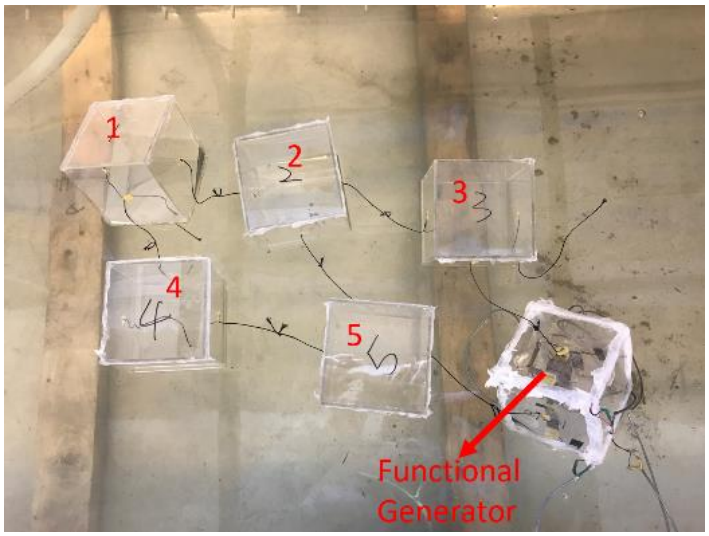

Figure. 51 Array test (Acceleration-based convertor)

In Fig.52, each curve represents the energy generated at each array position for different inter-unit distances. The convertors located in the middle of the array system (positions #2 and #5) always show the best power output in comparison to the rest of the converters. This is mainly due to the fact that the nature of the fluid flow behind the front-line positions #3 and #6 is significantly more turbulent. In addition, the converters in the middle of the array are always subjected to the in-phase reaction forces of the connections to front converters, which leaded to higher amplitude oscillations. From Fig. 53, the optimal distance between the units was determined to be one half of the wave length ~ 10cm. That means that optimal power output is achieved when each row

of converters is phase shifted by 180° which results in maximum relative displacement between converter's rows.

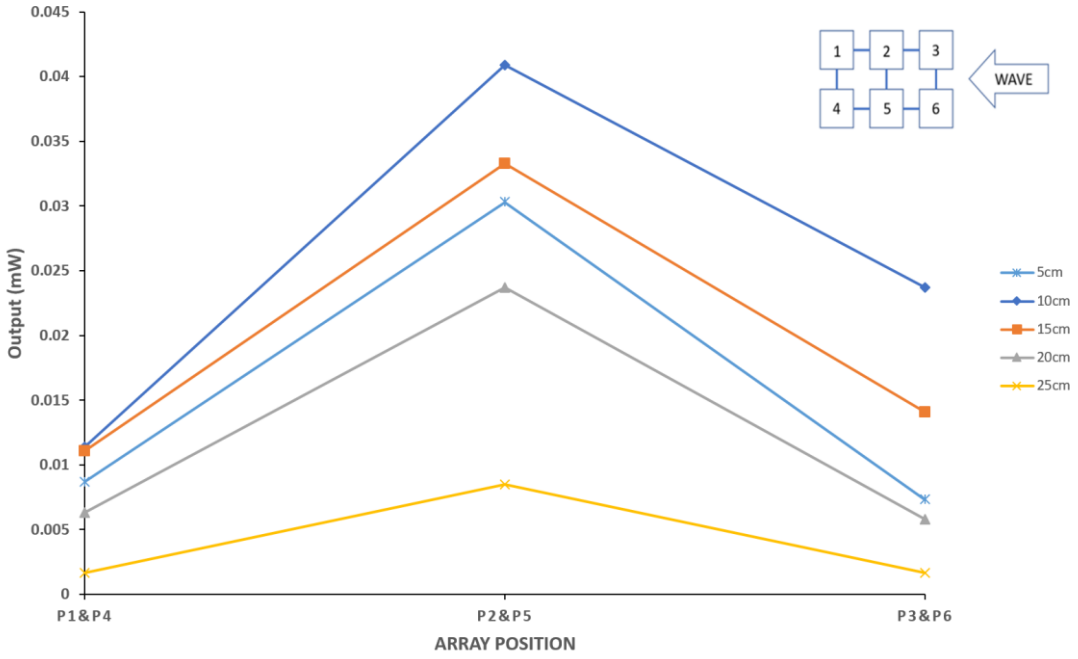

Figure 52. Output with different array position -Acceleration-based convertor.

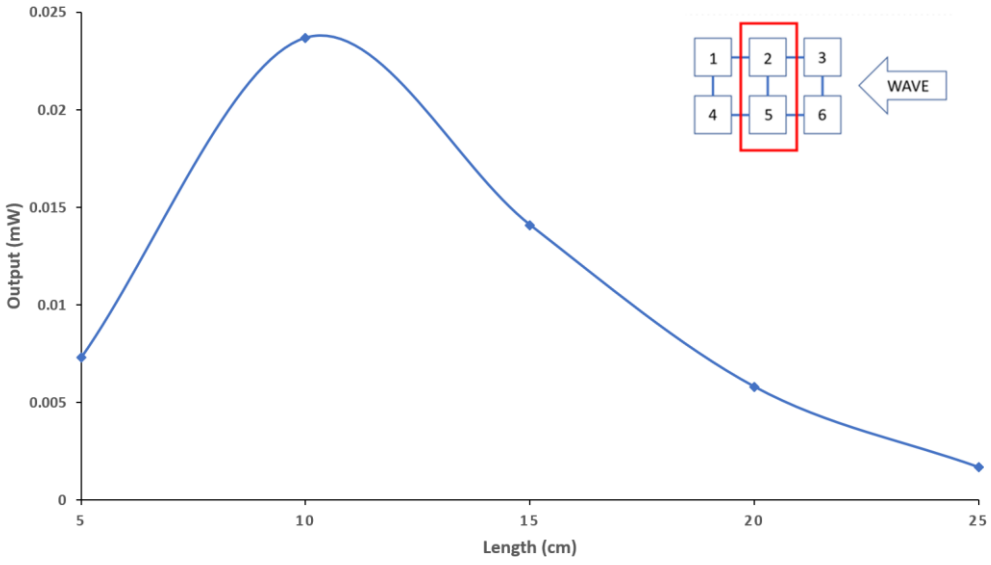

Figure 53. Output with different array distance -Acceleration-based convertor.

6.3.1 Deformation-based Array System

The deformation-based array system was built as a 3 × 2 convertors array (Fig. 54). The positions of the convertors in the array were varied, while the distance between the units was also adjusted from 10cm to 30cm in order to determine the optimal array configuration.

In Fig. 54, there were six convertors in total and one of them was functional. During the experiments, the position of the functional convertor was changed so that each array position was tested.

Figure 54. Array test (Deformation-based convertor)

The power output of the array is shown in Fig. 55. The power output of the units decreases, the further away they are from the wave impact. The front row converters position #3 and #6 showed the largest power output. Since the wave amplitude is affected by each row of converters, the last row of converters will be impacted by the wave with the smallest amplitude causing the smallest deformation in the array.

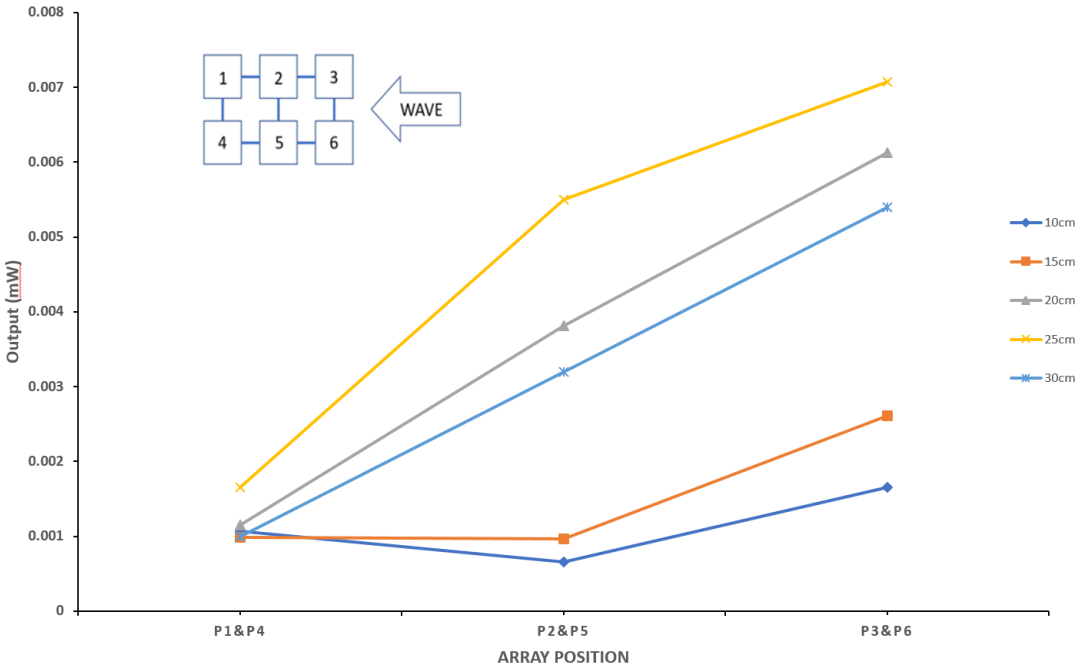

Figure 55. Output with different array position -Deformation-based convertor.

The optimal inter-unit distance equals to the approximate wave length ~25cm was obtained based on the results shown in Fig. 56. The inter-unit distance being equal to the wave length allows all units to be in-phase which leads to maximum deformation within the units.

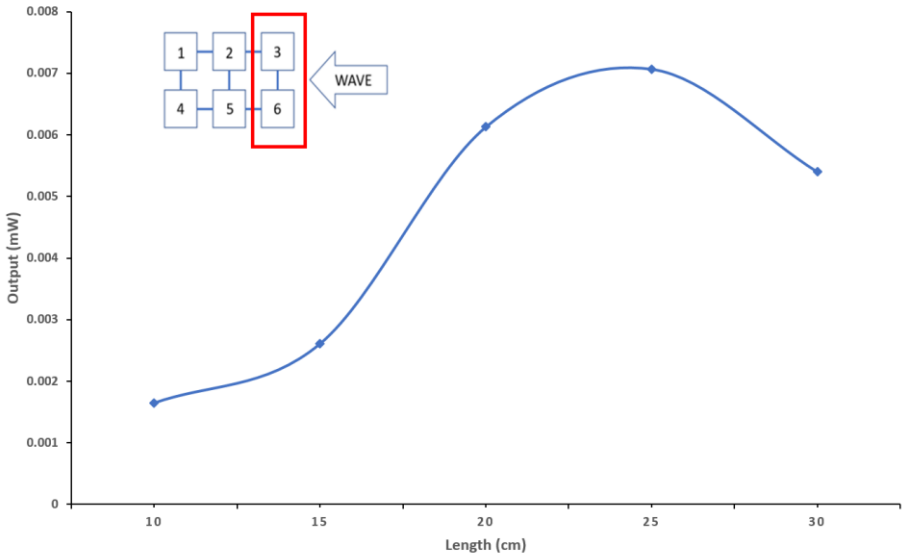

Figure 56. Output with different array distance -Deformation-based convertor

CHAPTER 7

Conclusions

Chapter 7 includes the conclusions drawn on the results obtained for both convertors concepts, as well as the corresponding array testing.

7.1 Acceleration-based Convertor

An acceleration based concept for energy harvesting from water waves was proposed and investigated. A detailed theoretical model of the system was developed. The theoretical model was used to determine the optimal convertor power output parameters such as spring stiffness, the mass ratio between the heavy mass and enclosure, and size of the enclosure. From the results, it can be concluded that the optimal mass ratio and convertor size are independent of wave environment. The value keeps constant with varying wave amplitude and frequency. With the optimal convertor geometry: spring stiffness - 10N/m, convertor size – 10cm and mass ratio – 0.65, a prototype of the acceleration-based converter was built for the field test. Four sets of field test were performed at multiple wave frequencies and amplitudes. The maximum power output of 5.0±0.6 mW was experimentally achieved at wave frequency and amplitude of 0.8Hz and 6cm. The numerical simulations at the same wave conditions predicted power output of 7.3±0.1mW, which overestimates the experimental results by 31%. The prototype was tested in the tank with controlled wave condition of 3cm and 0.5Hz. 100 groups data were recorded and the standard deviation was 0. 59mW. The low standard deviation meant the data were clustered around the average value and more reliable. It needs to be noticed that the overall power generated is between 5 - 6 mW under the condition of 0.8Hz and 6cm, which had better performance than the Disk Piezoelectric Wave Generator and Piezoelectric Cantilever mentioned in the literature

review. The energy generated for Disk Piezoelectric Wave Generator was 435.16mJ in 24hours, and the output for the 'Piezoelectric Cantilever' was 18mW with 40Hz frequency. [16, 17]

An array system for the energy harvester was developed. The optimal size of the array and the inter-unit length were experimentally determined. Based on the obtained results the optimal distance between the convertor units in the array is half whole wave length, which creates maximum relative displacement between the units. Such an array can easily be scaled up. Lake area of 1 km^2 can be covered with ~ 44 million convertors working in an array. If each converter produces 5mW, the overall array power output should ~ 220kW.

7.2 Deformation-based Convertor

An deformation based concept for energy harvesting from water waves was proposed and investigated. Two preliminary prototypes of the concept were developed and experimentally tested. The preliminary experimental results helped to select a concept with geometrical structure of a convertor with a jellyfish appearance. In addition, the preliminary test allowed to improve the performance of the 'jellyfish' by introducing the 'reverse jellyfish' concept. A theoretical model of the 'reverse jellyfish' was developed. The numerical simulations assisted to find the optimal size of the plate and the length of the piezoelectric strips. From the simulations, the optimal size of plate was determined to be 25cm and the strip length was optimized as 20cm. It indicated that the optimal heavy plate size and strips length are independent of wave environment while the overall output is related to the wave condition. A prototype of the 'reverse jellyfish' was field tested and maximum power output of 0.25±0.01 mW at the wave

environment of 0.8Hz and 7cm was achieved. The numerical prediction for the optimal wave conditions was 0.37±0.01mW overestimating the experimental value by 32.4%.

An array system for displacement based harvesters was developed and experimentally tested. The test results show that the optimal distance between the convertors is approximately equal to the wave length allowing the convertors in the array to oscillate in phase and providing maximum deformation within the array. Lake area of 1 km^2 area can be covered with 7.1 million displacement based converters connected in an array. The overall power output for such array would be 1.8 kW.

In regard to cost of the convertors, the acceleration-based convertor is twice more expensive (~$1000/conv) than the deformation-based convertor (~$500/conv). However, the power output of the array of acceleration-based convertors was around 122 times higher than the array of displacement-based convertors. Comparing the power output per capital investment between two types of convertors, the acceleration-based convertor has superior performance.

REFERENCES/BIBLIOGRAPHY

- Budynas, R. G. (n.d.). *Advanced Strength and Applied Stress Analysis.* McGraw-Hill Book Company.
- Greentumble. (2015, July 4). *Advantages and Disadvantages of Wave Power*. Retrieved from Greentumble: http://greentumble.com/advantages-and-disadvantages-of-wave-power/
- Hadzic, I., Hennig, J., Peric, M., & Xing-Kaeding, Y. (2005). Computation of flow-induced motion of floating bodies. *Applied Mathemtical Modelling, 29*, 1169-1210.
- Hawley, N., & Eadie, B. J. (2007). Observations of Sediment Transport in Lake Erie during the Winter of 2004-2005. *J. Great Lakes Res., 33*, 816-827.
- *How Hydrokinetic Energy Works*. (2008). Retrieved from Union of Concerned Scientists: http://www.ucsusa.org/clean-energy/renewable-energy/how-hydrokinetic-energy-works#bf-toc-1
- Jacobson , P. (2011). *Mapping and Assessmen of the United States Ocean Wave Energy Resource.* EPRI.
- Kempener, R., & Numann, F. (2014). *Wave Energy Technology Brief.* International Renewable Energy Agency.
- *Lake Erie Physical Data Sets*. (2004). Retrieved from NOAA Great Lakes Environment Research Laboratory: https://www.glerl.noaa.gov/res/projects/ifyle/data/data.mooring.html
- Lemay. (2010, May 22). *Oscillating Water Column*. Retrieved from Energy and the Environment - A Costal Perspective: http://coastalenergyandenvironment.web.unc.edu/ocean-energy-generating-technologies/wave-energy/oscillating-water-column/
- Li, W., Isberg, J., Engstrom, J., Waters, R., & Leijon, M. (2015). Parametric Study of the Power Absorption for a Linear Generator Wave Energy Converter. *Journal of Ocean and Wind Energy, 2*(4), 248-252.
- *Marine and Hydrokinetic Technology Glossary*. (n.d.). Retrieved from Office of Energy Efficiency & Renewable Energy: http://energy.gov/eere/water/marine-and-hydrokinetic-technology-glossary
- Mustapa, M., Yaakob, O., Ahmed, Y., Rheem, C., Koh, K., & Adnan, F. (2014). Wave energy device and breakwater integration: A review. *Renewable and Sustainable Energy Reviews, 77*, 43-58.

- *Ocean Wave Energy*. (n.d.). Retrieved from Bureau of Ocean Energy Management: https://www.boem.gov/Ocean-Wave-Energy/
- *PB3 PowerBuoy* . (n.d.). Retrieved from Ocean Power Technologies: http://www.oceanpowertechnologies.com/contacts/
- *Short history of piezoelectricity*. (n.d.). Retrieved from Applied Piezo: http://applied-piezo.com/short-history-of-piezoelectricity/
- *Small PVDF piezo film tabs*. (n.d.). Retrieved from Cold Gold: http://www.contactmicrophones.com/products-ftabs.html
- *Standard quick-mount bending generator*. (n.d.). Retrieved from Piezo System, Inc.: http://www.piezo.com/prodbg7qm.html
- Vinlol, C., Toma, D., Manuel, A., & Rio, J. d. (2013). Sea motion electrical energy generator for low-power applications. *2013 MTS/IEEE OCEANS-Bergen* (pp. 1-7). Bergen: IEEE.
- *Wave Energy Attenuator*. (n.d.). Retrieved from SmugMug: https://need-media.smugmug.com/keyword/Wave;attenuator
- *Wave Energy Converters*. (n.d.). Retrieved from Marine Biodiversity Wiki: http://www.marbef.org/wiki/Wave_energy_converters
- *Wave Energy Devices*. (n.d.). Retrieved from Alternative Energy Turorials: http://www.alternative-energy-tutorials.com/wave-energy/wave-energy-devices.html
- Woo, M., Back, K., Kim, J., Kim, S., Song, D., & Sung, T. (2015). Relationship between Current and Impedance in Piezoelectric Energy Harvesting System for Water Waves. *Journal of Electroceramics, 34*(2-3), 180-184.
- Woodford, C. (2017). *Piezoelectricity*. Retrieved from Explainthatstuff: http://www.explainthatstuff.com/piezoelectricity.html
- Xie, X., Wang, Q., & Wu, N. (2014). Potential of a piezoelectric energy harvester from sea waves. *Journal of Sound and Vibration, 333*(5), 1421-1429.

APPENDICES

Appendix A

MATLAB code of function file for the acceleration-based convertor simulation

```
function dxyz=Wave3d(t,xyz,g,rho_w,m,A,D0,w,f,k1,k2,H,M,D,l,L,C1,C2,C3)
    dxyz(1)=xyz(2);%x1
    dxyz(3)=xyz(4);%y1
    dxyz(5)=xyz(6);%x2
    dxyz(7)=xyz(8);%y2
    dxyz(9)=xyz(10);%z1
    dxyz(11)=xyz(12);%z2

    a=xyz(5)-xyz(1);
    b=xyz(7)-xyz(3);
    c=xyz(11)-xyz(9);

    %spring length
    %xy
    lc1xy=sqrt(a.^2+(H/2-b).^2);
    lc2xy=sqrt((H-a).^2+(H/2-b).^2);
    lc3xy=sqrt((H-b).^2+(a-H/2).^2);
    lc4xy=sqrt(b.^2+(a-H/2).^2);
    %yz
    lc3yz=sqrt((H-b).^2+(H/2-c).^2);
    lc4yz=sqrt(b.^2+(H/2-c).^2);
    lc5yz=sqrt((H-c).^2+(H/2-b).^2);
    lc6yz=sqrt(c.^2+(H/2-b).^2);
    %zx
    lc1zx=sqrt(a.^2+(H/2-c).^2);
    lc2zx=sqrt((H-a).^2+(H/2-c).^2);
    lc5zx=sqrt((H/2-a).^2+(H-c).^2);
    lc6zx=sqrt(c.^2+(a-H/2).^2);

    % forces' components
    %xy
    F1xxy=k1*(lc1xy-l)*(a/lc1xy);        F1yxy=k1*(lc1xy-l)*(H/2-b)/lc1xy;
    F2xxy=k2*(l-lc2xy)*(H-a)/lc2xy;      F2yxy=k2*(l-lc2xy)*(H/2-b)/lc2xy;
    F3xxy=k1*(lc3xy-l)*(a-H/2)/lc3xy;    F3yxy=k1*(lc3xy-l)*(H-b)/lc3xy;
    F4xxy=k1*(l-lc4xy)*(a-H/2)/lc4xy;    F4yxy=k1*(l-lc4xy)*b/lc4xy;
    %yz
    F3yyz=k1*(lc3yz-l)*(H-b)/lc3yz;      F3zyz=k1*(lc3yz-l)*(H/2-c)/lc3yz;
    F4yyz=k1*(l-lc4yz)*b/lc4yz;          F4zyz=k1*(l-lc4yz)*(H/2-c)/lc4yz;
    F5yyz=k1*(lc5yz-l)*(H/2-b)/lc5yz;    F5zyz=k1*(lc5yz-l)*(H-c)/lc5yz;
    F6yyz=k1*(l-lc6yz)*(H/2-b)/lc6yz;    F6zyz=k1*(l-lc6yz)*c/lc6yz;
    %zx
    F1xzx=k1*(lc1zx-l)*a/lc1zx;          F1zzx=k1*(lc1zx-l)*(H/2-c)/lc1zx;
```

```
    F2xzx=k2*(l-lc2zx)*(H-a)/lc2zx;        F2zzx=k2*(l-lc2zx)*(H/2-c)/lc2zx;
    F5xzx=k1*(lc5zx-l)*(H/2-a)/lc5zx;     F5zzx=k1*(lc5zx-l)*(H-c)/lc5zx;
    F6xzx=k1*(l-lc6zx)*(a-H/2)/lc6zx;     F6zzx=k1*(l-lc6zx)*c/lc6zx;

    %wave
    %y
     W1=D0*cos(f*xyz(3)-w*t);
    %z
     W2=D0*sin(f*xyz(9)-w*t);

    %Velocity
    %y
     B1=cosh(f*(D0*cos(f*xyz(3)-w*t)+D)./cosh(f*D));
     Vy=D0*w*B1*cos(f*xyz(3)-w*t);
    %z
     B2=sinh(f*(D0*sin(f*xyz(9)-w*t)+D)./cosh(f*D));
     Vz=D0*w*B2*sin(f*xyz(9)-w*t);

    %BOX
    %x-Direction
    dxyz(2)=g*rho_w*(A/m)*(D+W1+W2-xyz(1))-g+F1xxy/m+F2xxy/m+F3xxy/m-
F4xxy/m+F1xzx/m+F2xzx/m+F5xzx/m-F6xzx/m;
    %y-Direction
    dxyz(4)=-0.5*rho_w*A*(Vy-xyz(4)).^2*sign(xyz(4)-Vy)*1.05/m-
F1yxy/m+F2yxy/m-F3yxy/m-F4yxy/m-F3yyz/m-F4yyz/m-F5yyz/m+F6yyz/m;
    %Z-Direction
    dxyz(10)=-0.5*rho_w*A*(Vz-xyz(10)).^2*sign(xyz(10)-Vz)*1.05/m-
F1zzx/m+F2zzx/m-F5zzx/m-F6zzx/m+F3zyz/m+F4zyz/m-F5zyz/m-F6zyz/m;

    %MASS
    %x-Direction
    dxyz(6)=-g-F1xxy/M-F2xxy/M-F3xxy/M+F4xxy/M-F1xzx/M-F2xzx/M-
F5xzx/M+F6xzx/M-C1*(xyz(6)-xyz(2))/M;
    %y-Direction
    dxyz(8)=F1yxy/M-F2yxy/M+F3yxy/M+F4yxy/M+F3yyz/M+F4yyz/M+F5yyz/M-
F6yyz/M-C2*(xyz(8)-xyz(4))/M;
    %Z-Direction
    dxyz(12)=F1zzx/M-F2zzx/M+F5zzx/M+F6zzx/M-F3zyz/M-
F4zyz/M+F5zyz/M+F6zyz/M-C1*(xyz(12)-xyz(10))/M;

    dxyz=dxyz';
end
```

Appendix B

MATLAB code main script file for the acceleration-based convertor simulation

```
clear
clc
g=9.81;rho_w=1000;m=0.05;A=0.05;D0=0.11;w=2*pi*0.15;f=60;k1=10;k2=10;L=0.
1;H=0.1;l=0.04;M=0.132;D=1;C1=20;C2=20;C3=20;
options=odeset('RelTol',1e-7,'AbsTol',1e-7);
[t,xyz]=ode15s(@(t,xyz)Wave3d(t,xyz,g,rho_w,m,A,D0,w,f,k1,k2,H,M,D,l,L,C1,C2,
C3),[0 10],[D 0 0 0 D+H/2 0 H/2 0 D+H/2 0 H/2 0],options);
%box displacement
Disp_m=sqrt(xyz(:,1).^2+xyz(:,3).^2+xyz(:,9).^2);
figure(1)
plot(t,Disp_m)
%mass displacement
Disp_M=sqrt(xyz(:,5).^2+xyz(:,7).^2+xyz(:,11).^2);
figure(2)
plot(t,Disp_M-Disp_m)
%spring length
   a=xyz(:,5)-xyz(:,1);
   b=xyz(:,7)-xyz(:,3);
   c=xyz(:,11)-xyz(:,9);
   %xy
   lc1xy=sqrt(a.^2+(H/2-b).^2);
   lc2xy=sqrt((H-a).^2+(H/2-b).^2);
   lc3xy=sqrt((H-b).^2+(a-H/2).^2);
   lc4xy=sqrt(b.^2+(a-H/2).^2);
   %yz
   lc3yz=sqrt((H-b).^2+(H/2-c).^2);
   lc4yz=sqrt(b.^2+(H/2-c).^2);
   lc5yz=sqrt((H-c).^2+(H/2-b).^2);
   lc6yz=sqrt(c.^2+(H/2-b).^2);
   %zx
   lc1zx=sqrt(a.^2+(H/2-c).^2);
   lc2zx=sqrt((H-a).^2+(H/2-c).^2);
   lc5zx=sqrt((H/2-a).^2+(H-c).^2);
   lc6zx=sqrt(c.^2+(a-H/2).^2);
   %lc
   lc1=sqrt(lc1xy.^2+lc1zx.^2);
   lc2=sqrt(lc2xy.^2+lc2zx.^2);
   lc3=sqrt(lc3xy.^2+lc3yz.^2);
   lc4=sqrt(lc4xy.^2+lc4yz.^2);
   lc5=sqrt(lc5yz.^2+lc5zx.^2);
   lc6=sqrt(lc6zx.^2+lc6yz.^2);
   %Energy in spring
   E1=0.5*k1*(lc1-l).^2;
   E2=0.5*k2*(lc2-l).^2;
   E3=0.5*k1*(lc3-l).^2;
```

```
E4=0.5*k1*(lc4-l).^2;
E5=0.5*k1*(lc5-l).^2;
E6=0.5*k1*(lc6-l).^2;
E=E1+E2+E3+E4+E5+E6;
trapz(t,E)
```

Appendix C

MATLAB code of function file for the deformation-based convertor simulation

```
function
res=deWaveYVDAEDer(t,xy,dxy,g,rho_w,m,A1,A2,D0,w,f,M,D,l,V,Cd,L,h,Em)
%distance
   res(1)=dxy(1)-xy(2);%x1
   res(3)=dxy(3)-xy(4);%y1
   res(5)=dxy(5)-xy(6);%x2
   res(7)=dxy(7)-xy(8);%y2

%wave
   W1=D0*cos(f*xy(1)-w*t);%plate
   W2=D0*cos(f*xy(5)-w*t);%form

%Velocity x
    B1=cosh(f*(D0*cos(f*xy(1)-w*t)+D)./cosh(f*D));
    Vx1=D0*w*B1*cos(f*xy(1)-w*t);%plate

    B2=cosh(f*(D0*cos(f*xy(5)-w*t)+D)./cosh(f*D));
    Vx2=D0*w*B2*cos(f*xy(5)-w*t);%form


%Initial length
  %l1=0.03;
  l1=0.03 ;

%cross section area of floating form
   if (D+W2-xy(7))<0
      A3=0;
      dD2=0;
   else if (D+W2-xy(7))<h
      A3=(D+W2-xy(7))*l;
      dD2=D+W2-xy(7);
      else
         A3=l*h;
         dD2=h;
      end
   end


 %force buoyancy plate
 if (D+W1-xy(3))<0
    V=0;
 end;
 Fb=rho_w*g*V;
%Force drag
   Fd1=-0.5*rho_w*A1*(Vx1-xy(2)).^2*sign(xy(2)-Vx1)*Cd;%Plate
```

```
    Fd2=-0.5*rho_w*A3*(Vx2-xy(6)).^2*sign(xy(6)-Vx2)*Cd;%Floating Form


% F1,F2,F3,F4 force components
     F1x=xy(9)*(xy(5)-xy(1)-l1)/L;
     F1y=xy(9)*(xy(7)-xy(3))/L;

%base
    res(4)=dxy(4)-(-g+F1y./M+Fb/M); %y
    res(2)=dxy(2)-(Fd1./M+F1x./M); %x

%floating form Force
    res(8)=dxy(8)-(-g+rho_w*g*dD2.*A2/m-F1y/m); %y
    res(6)=dxy(6)-(Fd2/m-F1x/m); %x


%length constrain
    dl=(sqrt((xy(7)-xy(3)).^2+(xy(5)-xy(1)-l1).^2)-L);
%     if dl<0
%         Em=Em/2;
%     end
    res(9)=xy(9)-Em*dl;

    res=res';
end
```

Appendix D

MATLAB code main script file for the deformation-based convertor simulation

```
clear
clc
g=9.81;rho_w=1000;m=0.026;A1=0.00033;A2=0.0016;D0=0.07;w=2*pi*1;f=60;M=
0.092/1.5;l=0.04;L=0.17;V=0.000066;D=1;Cd=1.05;h=0.02;
Em=2e5;
a=sqrt(2)/2;
JMat =eye(9);
%algebriac equations
JMat(9,9)=0.0;

options = odeset('Reltol',1e-8,'Jacobian',{[],JMat});

yp0 = zeros(1,9);
%fixed variabels
yFixed = zeros(1,9);
%yFixed(1)=1;yFixed(3)=1;
%yFixed(5)=1;yFixed(7)=1;yFixed(9)=1;yFixed(11)=1;
%yFixed(17)=1;yFixed(19)=1;
%yFixed(23)=0;yFixed(24)=0;yFixed(14)=0;yFixed(16)=0;yFixed(18)=0;yFixed(20)
=0;

[y0,yp0] =
decic(@(t,xy,dxy)deWaveYVDAEDer2body(t,xy,dxy,g,rho_w,m,A1,A2,D0,w,f,M,D,
l,V,Cd,L,h,Em),0,[0 0 D-L-2*L 0 0.03 0 D-2*L 0 0],yFixed,yp0,[]);

%Mtest=[0 0 D-L 0 D-(L*a) 0 D-(L*a) 0 D-(L*a) 0 D-(L*a) 0 0.03+(L*a) 0
0.08+(L*a) 0 0.13+(L*a) 0 0.18+(L*a) 0 0 0 0 0]
% Mtest=[0 0 D-L 0 0.03 0 D 0 0]
% y0'


[t,xy]=ode15i(@(t,xy,dxy)deWaveYVDAEDer2body(t,xy,dxy,g,rho_w,m,A1,A2,D0,
w,f,M,D,l,V,Cd,L,h,Em),[0 20],y0,yp0,options);

plot(t,abs(xy(:,1)-xy(:,5)),t,abs(xy(:,3)-xy(:,7)))
x=mean((xy(:,9)) )
```

VITA AUCTORIS

NAME:	Wenzheng Cai
PLACE OF BIRTH:	Shanghai, China
YEAR OF BIRTH:	1992
EDUCATION:	Dajing High School, Shanghai, China, 2010
	University of Windsor, B.App.Sc., Windsor, ON, 2015